Pacific Gas and Electric Company

Lawrence F. Womack
Vice President
Nuclear Services

Diablo Canyon Power Plant
P.O. Box 56
Avila Beach, CA 93424

805.545.4600
Fax: 805.545.4234

June 7, 2004

PG&E Letter DCL-04-071

U.S. Nuclear Regulatory Commission
ATTN: Document Control Desk
Washington, DC 20555-0001

Docket No. 50-275, OL-DPR-80
Docket No. 50-323, OL-DPR-82
Diablo Canyon Units 1 and 2
Update to the Seismicity Evaluation of the December 22, 2003 San Simeon Earthquake

Dear Commissioners and Staff:

Pacific Gas and Electric Company (PG&E) submits the attached report in response to the Nuclear Regulatory Commission (NRC) requests to evaluate the relevance of the December 22, 2003 San Simeon earthquake to the seismotectonic evaluation of the Central California coast region performed for the Long Term Seismic Program (LTSP) for the Diablo Canyon Power Plant. This report provides the results of further analysis of the seismicity of the event that was presented in the March 29, 2004 letter to the NRC, Supplement to Special Report 03-04: San Simeon Earthquake of December 22, 2003 (PG&E Letter DCL-04-031), with additional information on the geology and field reconnaissance.

If you have any questions, please contact me at 805-545-4600, or Mr. Lloyd Cluff at 415-973-2791.

Sincerely,

Lawrence F. Womack
Vice President Nuclear Services

swh/A0597040 AE04
Enclosure
cc: Bruce S. Mallett, Region IV
David L. Proulx, Resident
Girija S. Shukla, NRR
Diablo Distribution

A025

Update to the Seimicity Evaluation of the December 22, 2003 San Simeon Earthquake

1.0 Introduction

The purpose of this report is to respond to the Nuclear Regulatory Commission (NRC) request to evaluate the relevance of the December 22, 2003 San Simeon earthquake to the seismotectonic evaluation of the central California coast region done for the Long Term Seismic Program (LTSP) for the Diablo Canyon Power Plant. The information presented in this report is an update of the seismicity presented in the March 29, 2004 letter to the NRC, "Supplement to Special Report 03-04: San Simeon Earthquake of December 22, 2003" (PG&E Letter DCL-04-031), with additional information on the geology and field reconnaissance.

2.0 Tectonic Setting

The San Simeon region is an area of active tectonic deformation between the Pacific Plate and the Sierra Nevada-Central Valley microplate driven primarily by right shear between the two plates (Figure 2-1). The San Andreas transform fault that strikes N40°W with a slip rate of 35 ± 3 mm/yr (right lateral) forms the main plate boundary. Other faults also accommodate deformation between the plates in this area: the right slip San Simeon-Hosgri fault zone, the right-slip Rinconada fault, and the oblique slip (reverse-right lateral) Oceanic-West Huasna fault.

PG&E (1988; Lettis et al., in press) divided the region into several crustal domains undergoing distinct styles of deformation: the Los Osos domain; the Southern Coast Ranges domain (including the Santa Lucia Mountains); the Western Transverse Ranges domain; and the offshore Santa Maria Basin domain (Figure 2-2). The triangular-shaped Los Osos domain is bounded on the west from the structurally detached offshore Santa Maria Basin domain by right-lateral strike slip faulting on the near vertical Hosgri-San Simeon fault zone; on the northeast from the Southern Coast Ranges domain by reverse and reverse-oblique slip faulting along the northeast-dipping Oceanic-West Huasna fault zone; and on the south from the western Transverse Range domain by reverse-left oblique slip faulting along the Santa Ynez River fault.

2.1 Los Osos Domain

Northeast-southwest-directed crustal shortening in the Los Osos domain is caused primarily by clockwise rotation of the Western Transverse Ranges (PG&E, 1988; Lettis and others, in press). Crustal shortening within the Los Osos domain is accommodated by a series of west-northwest-trending reverse and oblique slip faults that border areas of intervening subsidence and uplift (Figure 2-2). The Diablo Canyon Power Plant is on the west side of one of these uplifts, the San Luis Range that is a structural block bordered by the Los Osos fault on the northeast and Southwest Boundary fault zone on the southwest. Based on the elevation of marine terraces that border the San Luis Range, the rate of uplift of the range is 0.1 to 0.2 mm/yr (PG&E, 1988). Detailed paleoseismic studies on the Los Osos fault and Southwest Boundary fault zone indicate reverse slip rates of 0.2 mm/yr to 0.4 mm/yr and 0.06 to 0.11 mm/yr, respectively (PG&E, 1988).

2.2 Southern Coast Range Domain

Uplift of the Southern Coast Ranges domain is the result of several interrelated processes: including northeast-southwest-directed crustal shortening imparted to the Southern Coast Ranges from the bordering Los Osos domain (discussed above); progressive left-restraining transfer of dextral shear across the Southern Coast Ranges from the San Gregorio-San Simeon-Hosgri fault system on the west to the southern Rinconada fault on the east; and a large left-restraining bend within the San Gregorio-San Simeon-Hosgri faults system centered on the San Simeon fault zone. These three processes combine to produce northeast-southwest-directed crustal shortening within the Santa Lucia Range portion of the Southern Coast Ranges domain.

In the San Simeon region a large component of this crustal shortening and uplift appears to be accommodated by reverse and reverse-oblique slip along the Oceanic-West Huasna fault zone that is reflected in the mountain ranges in the hanging wall of the fault. Based on the elevation of uplifted marine terraces along the Santa Lucia Range, north of the intersection of the Oceanic fault with the San Simeon fault, the rate of reverse slip on the northern part of Oceanic fault is greater than 0.5 mm/yr (PG&E, 1988) and may be more than 1 mm/yr depending on the down-dip geometry of the fault.

3.0 Geologic Setting

The major geologic units shown in the San Simeon region (Jennings, 1958) include the following (Figure 3-1):

1. Mesozoic-Tertiary Franciscan complex;
2. Coast Range ophiolite;
3. Late Cretaceous to Paleogene marine strata;
4. Miocene Monterey Formation;
5. Pliocene-Pleistocene fluvial deposits; and
6. Quaternary marine terrace and alluvial fan deposits

In this region the Quaternary deformation is superimposed on older Mesozoic and early Tertiary structures, such as the Nacimiento fault, which formed when this region was part of a convergent margin between the Pacific plate and North American plate. The closest late-Quaternary fault to the epicenter of the 2003 San Simeon earthquake is the Oceanic-West Huasna fault, which is described below.

3.1 Oceanic-West Huasna Fault

The Oceanic-West Huasna fault is a late Quaternary fault (Jennings, 1994) that extends 120 kilometers southeast from San Simeon to Santa Maria (Figure 2-1). The fault lies along the base and within the mountain front of the Santa Lucia Range and dips northeast about 45 to 60 degrees based on mine adit data and geologic cross sections (PG&E, 1989). The map trace consists of three distinct segments with different strikes, the northern and central segments that are called the Oceanic fault, and southern segment that is called the West Huasna fault. The northern segment is about 28 kilometers long, strikes N62°W and the map pattern indicates that it dips about 60 degrees to the northeast. The central segment is about 40-kilometer long, strikes

N45°W and the map pattern indicates that it dips 70 to 80 degrees east. The southern segment is 50 kilometers long, strikes N30°W and the map pattern indicates that it dips steeply east to near vertical.

The San Simeon earthquake occurred near the northern segment of the Oceanic fault where the surface expression of the fault is poor and has several strands. In this area the Oceanic fault locally juxtaposes Franciscan complex up on the east against Monterey Formation on the west (Hall, 1974) (Figure 3-1), thus providing direct stratigraphic evidence for post-Miocene reverse offset on the Oceanic fault.

4.0 Geological Observation following the 2003 San Simeon Earthquake

Following the 2003 San Simeon Earthquake, we performed aerial and field reconnaissance of the epicentral region on January 15 and 16, 2004. Our reconnaissance included a helicopter over flight and field checking at selected points on the ground to document any ground deformation from the earthquake.

4.1 Findings

The aerial and field reconnaissance covered the epicentral region of the earthquake, the Oceanic fault north of San Luis Obispo, and the on-shore portions of the San Simeon and Los Osos faults. The surface expression of the Oceanic fault is poor (Photos 1 and 2). We observed no evidence of surface faulting along the surface trace of the Oceanic fault as mapped by Hall (1974, 1978), a finding in agreement with the US Geological Survey reconnaissance (Hardebeck and others, 2004; Treiman and others, 2004). In particular, we found no offsets across paved roads, including Old Creek Road, Highway 46, and the access road to Hearst Castle, that cross the fault, nor did we observe any scarplets or cracks along the fault traces; such features would have been easily seen because the grass was short and cattle trails, as well as offsets of a few inches at the heads of incipient landslides, were readily evident. Hardebeck and others (2004) estimate from their helicopter reconnaissance that any offsets greater than 10-15 cm along the fault would have been evident. We believe that we would have seen offsets somewhat smaller, 5 to 10 cm.

In addition, no surface faulting was observed along the San Simeon or Los Osos faults, indicating that these faults did not experience any sympathetic movement during the San Simeon earthquake. Similarly, Hardebeck and others (2004) did not report any surface displacement on the Nacimiento fault and Blanck (2004a,b) reported no rupture on the San Simeon and Cambria faults.

Slope failures were common in and southeast of the epicentral area, agreeing with the observations mentioned by Hardebeck and others, (2004). Rockfalls occurred below many of the steep rock cliffs and below rocky outcrops. Ground cracks and incipient failures of many landslides were evident on both sides of the Santa Lucia Range (Photos 3 and 4). One example that we examined is at the ridge above the Smith Ranch, north of Old Creek Road. At this location, which is on one of the traces of the Oceanic fault, cracks up to 4 inches high formed an arcuate scarplet that marked incipient reactivation of an older, dormant landslide.

We also found an apparent sackungen (ridge-top cracks) paralleling a ridgecrest on the Hartzel Ranch south-southeast of the junction of Highway 46 and Old Creek Road (Photo 5). This feature consists of several en echelon cracks that form a zone 200 to 300 yards long and strike northerly. The cracks are in serpentine bedrock and are up to 4 inches wide and have vertical offsets up to 4 inches. The cracks mark a shallow graben about 50 feet wide that sub-parallels and crosses the south-trending ridgecrest where the farm access road traverses the ridge. The southeastern cracks at the south of the farm road have down-on-the-west displacement, but show no arcuate pattern as they cross the colluvial-covered slope south of the road. The northwestern cracks follow the general ridge crest and have offsets down on the east.

5.0 Seismicity

The M_W 6.5 San Simeon earthquake of 22 December 2003 initiated a prolific aftershock sequence that continues to produce earthquakes. As of 12 May 2004, the USGS online database (USGS, 2004) reports over 5600 aftershocks greater than about magnitude (M) 0.8 have occurred since the main shock, including 3200 M 1, 1800 M 2, 180 M 3 and 18 M 4 earthquakes. To date, there has not been a M 5 aftershock. This section of the report presents analyses of the main shock and 120 M 3 and greater aftershocks to 18 March 2004, including 13 M 4 earthquakes, that were recorded by both the USGS and PG&E seismic networks. Figure 5-1 shows the USGS aftershock locations with the locations of the main shock and selected aftershocks in this study. The results of our analyses were presented on 15 April 2004 at the 2004 Annual Conference of the Seismological Society of America (McLaren and Stanton, 2004).

We describe the data processing to obtain well-determined locations and focal mechanisms; the results are displayed in map and cross section views. We compare our results to historic earthquakes and earthquakes from the 1987 to 1997 data set from the San Simeon region analyzed by McLaren and Savage (2001). We also compare our main shock hypocenter results to a preliminary teleseismic body-wave study by Ichinose and Somerville (2004).

The PG&E and USGS short period seismographic stations are shown in Figure 5-2. The PG&E network was installed in 1987 as part of the PG&E Long Term Seismic Program (PG&E, 1988) to improve the accuracy of the earthquake locations by improving the station coverage of the USGS network. The PG&E network consists of 20 analog stations; 15 high gain vertical-only stations and 5 dual high and low gain 3-component stations. The 3-component stations help to constrain the earthquake depths (hypocenters). The data are transmitted continuously via PG&E microwave telemetry to a central recorder in San Francisco.

5.1 Data processing

Data processing is described for the earthquake locations and focal mechanisms. New magnitudes were not re-estimated for the events. The moment (M_W) magnitude for the main shock and local (M_L) magnitudes for the aftershocks are from the USGS online catalog (USGS, 2004).

The main shock and selected M 3 and greater aftershocks were located using the program Hypoinverse 2000, a Y2K version of Klein (1989), which inverts P- and S-wave arrival times

using a least squares hypocenter determination algorithm. A linear gradient version of the 1-D flat layer velocity model and station corrections from McLaren and Savage (2001) (provided by Dr. F. Klein, USGS) was used in the inversion. The linear gradient velocity model generally results in improved travel time RMS values (a measure of how well the velocity model worked) because it smoothes out the discontinuities in travel time derivatives which can result from using a flat layer model. Other location parameters are a P- to S-wave velocity ratio (V_P/V_S) of 1.73, a distance cutoff at 75 km, and a starting depth of 7 km depth.

The final PG&E data set consists of 121 earthquakes; the San Simeon earthquake main shock, 13 M 4 and 107 M 3 aftershocks. The earthquake location parameters are listed in Table 5-1. The location errors in Table 5-1 indicate that these earthquakes are well constrained. The average horizontal and vertical errors are less than 1 km, 0.20 ± 0.05 km and 0.66 ± 0.34 km, respectively. The average number of P- and S- wave readings per earthquake used in each location is 56; the average number of S-waves used is 3. The average root mean square (RMS) of the P- and S-wave residual travel times, is 0.11 ± 0.02; and the average azimuthal gap between stations is 62 degrees (i.e., the stations are generally well distributed around each earthquake).

The main shock hypocenter was constrained using the S-P time from the CGS Cambria strong motion station at the PG&E Cambria station. The two stations are nearly the same distance (less than one km difference) from the epicenter. This was fortuitous because most of the S-wave readings from the close-in 3-component stations were clipped to about 15 km distance from the aftershock epicenters.

Focal mechanisms were estimated from the Hypoinverse output using FPFIT2, a Y2K version of FPFIT by Reasenberg and Oppenheimer (1985). The final dataset of 97 focal mechanisms are constrained by misfit values less than 0.25, at least 20 first motions, and mechanisms that converge to a solution. For multiple solutions, the one with the lowest misfit value was chosen.

5.2.1 San Simeon main shock

The main shock location is 35°N41.88, 121°W6.21 at a depth of 11.3 km (McLaren and Stanton, 2004). The location errors show that the earthquake location is well constrained (Table 5-1). The Cambria station, where the S-P time was applied, is at a distance of 10.9 km from the epicenter. This is well within the 1.4 times the focal depth distance that Gomberg et al (1990) concluded was the maximum distance one should use S-wave readings to confidently constrain the focal depth. Our depth is consistent with the 12 km depth determined by Ichinose and Somerville (2004) using teleseismic body-wave data and the 1D velocity model by McLaren and Savage (2001) for the source model. Hardebeck et al (2004) reported a depth of 7.1 km for the main shock using the double-difference location method with the McLaren and Savage (2001) velocity model. Preliminary tests using the PG&E/USGS integrated data and the previous integrated data from McLaren and Savage (2001) as input into the double-difference program has produced more consistent results (10.6 km depth for the main shock).

Figure 5-3 compares the San Simeon earthquake location with previous earthquakes of magnitude 5 and greater. As evident from the figure, magnitude 5-6 earthquakes are relatively common in the San Simeon region, along the northwest trending Santa Lucia Range. The main

shock occurred about 20 km southeast from the 1952 Bryson earthquake, a M_L 6.2 event (Savage and McNally, 1974) that occurred a few km west of the Nacimiento fault (Dehlinger and Bolt, 1987). Until 2003, this had been the largest earthquake to occur in the San Simeon region. A M5 to 6 earthquake in 1853 also occurred in the San Simeon region. However, the 1853 location of Toppozada et al (1981) is poorly constrained; it could have occurred near the Bryson earthquake or offshore to the west (McLaren and Savage, 2001). Two more recent M5 events along this northwest trend are the 1983 M_L 5.4 San Simeon and the 1991 M_L 5.1 Ragged Point earthquakes.

The detailed output from FPFIT2 in Figure 5-4 shows the main shock focal mechanism and mechanism parameters. The mechanism is reverse motion along a northwest trending fault plane that strikes 297° and dips 61° NE with a 96° rake. It is well constrained with a misfit value of 0.08 and little scatter of the P and T axes (small circle plot, lower right corner).

The main shock focal mechanism is compared with the mechanisms of previous earthquakes in Figure 5-5. Both the 1952 Bryson strike slip focal mechanism and the 2003 San Simeon reverse mechanism are consistent with other strike slip, oblique slip and reverse slip mechanisms that events that have occurred in the region, and are consistent with NE-SW directed compression.

5.3 Seismicity patterns

The aftershocks extend 35 km southeast from the main shock. The majority of the aftershock epicenters are located between the mapped surface traces of the Oceanic and Nacimiento faults. There are three main clusters of the M 3 and greater earthquakes within the aftershock pattern, and they are consistent with the patterns of the smaller earthquakes (Figure 5-1). Two clusters are at the northwest end, one is northeast and one is southwest of the main shock. The third cluster is at the southeast end of the aftershock zone. The clusters are hereafter called the northeast, southwest and southeast clusters, respectively. The northeast and southwest clusters near the main shock are more tightly clustered than the diffuse southeast cluster.

Figures 5-6 and 5-7 show the San Simeon main shock and M 3 and greater aftershocks in map and cross section views combined with a previous data set of earthquakes from 1987 to 1997 by McLaren and Savage (2001). In map view (Figure 5-6) and cross section view AA' (Figure 5-7) the San Simeon earthquake locations are near the previous clusters of the 1987-1997 data. However, aftershocks shown in cross section AA' between distance points 25 and 30 locate between the two clusters of the previous data.

Table 5-1 lists the cluster location for each event. There are nearly the same amount of earthquakes in the southwest cluster as in the southeast cluster (47 and 48, respectively). Most of the M 4 events are in the northeast and southwest clusters.

Figure 5-6 shows the 13 M 4 earthquake locations numbered as they occurred in time. Events 1 through 8 occurred in the first 24 hours and show that the three clusters formed nearly immediately after the main shock. Over the time period of this report the events have continued to alternate in location from cluster to cluster. The M 3 earthquakes (Table 5-1) similarly show this alternating cluster pattern.

In cross section view the main shock plots at the base of the seismogenic zone (Figure 5-7, cross sections AA' and BB') defined by the previous 1987-1997 data, and the aftershocks extend from near the main shock depth to a few kilometers beneath the surface. The aftershock patterns in cross section AA' shows that, except for the M 3 aftershocks between distance markers 25 to 30 km, the aftershocks occur where there has been previous clustered activity. The zone between distance points about 20 to 30 km and depths between 5 to 10 km has been modeled as the area of maximum slip initiated by the San Simeon earthquake (e.g. Dreger, 2004; Ji, 2004; Ichinose and Somerville, 2004), and is centered near the change in strike of the Oceanic fault (Figure 5-6).

Cross section BB' shows that aftershocks between the main shock and the surface trace of the Oceanic fault loosely define a northeast dipping plane. Earthquakes west of or beneath the 60°, northeast dipping plane shown in the cross section, suggest that if the earthquake occurred on the Oceanic fault, the fault zone may be a wider zone than the single trace mapped at the surface shown in Figure 5-7. Earthquakes northeast of the main shock show a fairly distinct southwest dipping trend; perhaps defining a backthrust. The patterns of the previous data do not define specific fault planes.

Cross section CC' (Figure 5-7) across the southeast cluster shows diffuse patterns for both the aftershocks and previous data, with a diffuse vertical aftershock pattern above distance point 15. The diffuse patterns suggest complex faulting in this area. The three M 4 events are possibly aligned along a steeply northeast dipping plane, however the M 3 aftershocks do not lie near the plane.

5.4 Focal mechanism patterns

Figure 5-8 shows a) the focal mechanisms of the main shock and 96 aftershocks and b) focal mechanisms from the previous 1987 to 1997 data. The majority of the aftershock mechanisms in the two northwest clusters are reverse, similar to the main shock mechanism (Figure 5.8a). Many of the mechanisms in the southeast cluster are also reverse motion, however, there is more variation. Several of the events have normal and normal oblique mechanisms, consistent with complex faulting. The fault planes of the normal mechanisms strike nearly north-south, as opposed to the northwest trend of the reverse mechanism fault planes. These same patterns are also seen in the previous data (Figure 5.8b), including the southeast region where mechanisms are also varied.

Figure 5-9 shows the focal mechanisms projected on to cross sections BB' and CC'. In cross section BB' the line angled at 60 ° is the preferred fault plane of the main shock. It projects to the surface near the mapped surface projection of the Oceanic fault. The mechanisms west of the main shock in the deeper part of the section (between about 5 and 10 km depth) show mostly reverse motion, while events in the shallower section near the surface trace of the Oceanic fault have more strike slip motion. Mechanisms northeast of the main shock show primarily southwest reverse fault motion, and are consistent with back thrusting along the Nacimiento fault zone. The mechanisms in cross section CC' of Figure 5-9 reiterate the variety and complexity of the faulting in this area. Several of the fault planes show vertical to nearly vertical fault motion, consistent with the diffuse vertical patterns.

5.5 Earthquake Stress Transfer

Hardebeck et al. (2004) discuss whether the 2003 San Simeon earthquake may trigger earthquakes on other faults in the area, separate and distinct from those aftershocks occurring along the Oceanic-West Huasna fault zone. Figure 5-10 shows the Coulomb stress changes produced by the San Simeon earthquake, as resolved on vertical strike-slip fault planes parallel to the San Andreas fault (N40W), and all seismicity in the region following the December 22 event. Stress increases on the order of 0.1- 1 bar (red areas in Figure 5-10) estimated for the region between the San Andreas and Rinconada faults, and the offshore San Simeon fault are coincident with a relatively higher concentration of seismic activity compared to those areas with stress reductions (blue areas). Note that the earthquakes plotted in Figure 5-10 represent reverse, normal, as well as strike–slip faulting and may not be appropriate for comparison with this particular Coulomb stress change model. The absence of seismic activity along the Hosgri fault zone, a vertical strike slip fault that strikes sub-parallel to the San Andreas, may reflect its location in a zone of static stress reduction associated with the San Simeon event.

6.0 Ground Motions

Strong ground motions recorded at distances less than 30 km from the main shock were significantly smaller than predicted by commonly used ground motion attenuation relations, including the ground motion models used as part of the LTSP evaluations (Figure 6-1)

In particular, the free-field response spectral values at frequencies greater than 0.5 Hz recorded at the DCPP site were lower than the median response spectral values computed for this earthquake using attenuation relations similar to those used in the LTSP (Figure 6-2). Part of the reason for the lower ground motions at DCPP is that the power block is located on rock with a shear-wave velocity of 1300 – 1500 m/s, but the attenuation relations used in the LTSP were based on ground motions primarily recorded on soft-rock and shallow soil sites (shear wave velocity of about 475 – 600 m/s). Sites with larger shear-wave velocities tend to have smaller ground motions since there is less of an impedance contrast.

Hardebeck et al. (2004) compare the recorded peak accelerations with the Boore et al (1997) attenuation relation for a V_{S30} (average shear-wave velocity over the top 30 m) of 700 m/s (e.g. assuming all of the sites are rock sites). They find that the Boore et al model agrees reasonably well with the observed peak acceleration over the distance range of 10 to 80 km. The Boore et al model gives much lower peak acceleration than the attenuation relation used in the LTSP for rock sites (Sadigh et al, 1997; Figure 6-3), so the agreement between the Boore et al model for rock and the recorded peak accelerations from the San Simeon earthquake is consistent with the observation that the ground motions are lower than the median ground motion using attenuation relations from the LTSP.

New attenuation relations incorporating ground motions from recent earthquakes are currently being developed as part of the Pacific Earthquake Engineering Research Center (PEER) Lifelines Next Generation Attenuation (NGA) project. The NGA project will lead to new comprehensive models for ground motion attenuation that will include evaluations of directivity effects, style-of-

faulting effects, hanging wall/footwall effects, and buried vs. shallow slip effects. These new models are expected to be completed in October 2004.

7.0 NRC topics for consideration

The NRC has asked PG&E if the San Simeon earthquake will effect the source characterization or ground motion attenuation characterization used in the LTSP (NRC email, 2004). Specific topics for consideration are: 1. Maximum magnitudes assigned to earthquake sources; 2. Source zone configurations and geometries; 3. Earthquake recurrence rates, 4. Probability of activity assigned to faults and source zones; 5. Appropriateness of attenuation relationships for estimating ground motions; and 6. Considerations given to the possibility for thrust faulting on the Hosgri fault.

1. Maximum magnitudes assigned to earthquake sources -
   The rupture dimension of the San Simeon earthquake is approximately 35 km x 14 km. Using this rupture dimension, the expected magnitude based on LTSP models of magnitude vs. length and magnitude vs. area for reverse faults range from M6.8 to M7.2. Since these estimated magnitudes are greater than the M6.5 of the San Simeon earthquake, the occurrence of the San Simeon earthquake does not indicate a need to increase the maximum magnitudes used in the LTSP.

2. Source zone configurations and geometries -
   PG&E's estimate of the hypocentral depth of the San Simeon earthquake of 11 to 12 km is consistent with the through-going high angle fault model used for the Oceanic fault in the LTSP. Other researchers have reported shallower hypocentral depth estimates (e.g. 7-8 km) that are consistent with a detachment fault model, but these other estimates have not fully incorporated the joint PG&E USGS data sets for locating the hypocenter. The hypocentral depth is important because a deep hypocentral depth is not consistent with the detachment fault model. Based on PG&E's depth estimate, there is no need to revise the source geometries based on the occurrence of the San Simeon earthquake; however, additional work on the hypocentral depth is needed to reach consensus with USGS researchers.

3. Earthquake recurrence rates -
   The occurrence of a single earthquake sequence does not have a significant effect on recurrence rates for a PSHA. No revision to earthquake recurrence rates used in the LTSP is needed based on San Simeon earthquake.

4. Probability of activity assigned to faults and source zones -
   The Oceanic fault is considered active in the LTSP and by the California Geological Survey (CGS). The occurrence of the San Simeon earthquake does not affect probability of activity assessments of faults in the LTSP.

5. Appropriateness of attenuation relationships for estimating ground motions -
   Free-field ground motions recorded at DCPP from the San Simeon earthquake were much smaller than expected. The lower ground motions may reflect effects of hard rock

conditions at DCPP as compared to the generic "rock" used in ground motion models. The ongoing NGA project conducted at PEER is developing new attenuation relations that incorporate new strong motion data from recent large magnitude earthquakes (since 1995). The appropriateness of the attenuation relations used in the LTSP will be evaluated once the results of the NGA project are available.

6. Considerations given to the possibility for thrust faulting on the Hosgri fault - The LTSP considered alternative styles-of-faulting for the Hosgri fault: 65% strike-slip, 30% reverse/oblique, and 5% reverse. In SSER-34, the NRC combined reverse/oblique and reverse and used 2/3 strike-slip and 1/3 reverse-reverse/oblique. Focal mechanisms from recent seismicity (after 1987) show mainly strike-slip mechanisms along the Hosgri fault (McLaren and Savage, 2001 figure 9). Since the recent seismicity is consistent with the strike-slip characterization of the Hosgri fault, there is no need for increasing the weight of reverse style-of-faulting on the Hosgri fault.

8.0 Conclusions

- No surface rupture occurred from the San Simeon earthquake or on any other potentially causative faults within the Santa Lucia Range. No sympathetic movement was observed on nearby regional faults, including the San Simeon, Los Osos, or Southwest boundary zone faults. Potential surface rupture associated with the earthquake was not large enough to propagate to the ground surface.

- Review of the geology along the Oceanic-West Huasna fault for this report confirms the Oceanic fault is a northeast-dipping thrust/reverse fault.

- The Oceanic fault as a reverse fault was recognized and incorporated into the tectonic model developed by PG&E in the LTSP.

- Using a combination of PG&E and USGS data, PG&E estimates a hypocentral location of the San Simeon main shock at 35°N41.88, 121°W6.21, 11.3 km depth, and a reverse focal mechanism, 297° strike, 61° NE dip, 96° rake. This depth is consistent with the 12 km depth of the earthquake estimated from teleseismic body-wave data.

- The main shock and aftershock locations are in a region where previous reverse motion earthquakes have occurred.

- Near the main shock, the northeast dipping fault plane of the aftershock patterns and reverse mechanisms, and the 61° northeast dip on the main shock focal mechanism are consistent with the Oceanic fault as the source of the earthquake.

- The main shock strong ground motions recorded at the Diablo Canyon Power Plant were significantly smaller than predicted by commonly used ground motion attenuation relations including the ground motion models used as part of the LTSP evaluations.

- The occurrence of the San Simeon earthquake is consistent with the tectonic framework used in the LTSP. Based on preliminary evaluations, the occurrence of the San Simeon earthquake does not indicate that significant changes need to be made to the source characterization used in the LTSP. The ground motions from the San Simeon earthquake indicate that the LTSP ground motion models may overestimate the high frequency ground motion at DCPP. A detailed evaluation to address these topics will be completed in late 2004.

9.0 Acknowledgements

This report was prepared under the direction of Lloyd Cluff, Director, PG&E Geosciences Department (Geosciences). The tectonic and geologic sections were prepared by William Lettis, Principal Geologist, William Lettis & Associates, Inc. (WLA), William D. Page, Senior Seismic Geologist (Geosciences), and Jeffrey Unruh Principal Geologist (WLA). The Seismicity sections were prepared by Marcia McLaren, Seismologist (Geosciences). The ground motion section was prepared by Norm Abrahamson, Senior Seismologist (Geosciences). The text was reviewed by Stu Nishenko, Senior Seismologist (Geosciences).

The helicopter reconnaissance was performed by Lloyd Cluff, William Lettis, William Page and Lew Rosenberg, San Luis Obispo County Geologist. Lettis and Page, and in places Rosenberg, made the ground reconnaissance. We thank the ranchers, Mr. Smith and Mr. Jim Hartzel, who kindly showed us geologic features on their properties and discussed the impact of the earthquake on their operations with us.

Fruitful discussions concerning the geologic and seismologic issues raised by the earthquake were had with numerous geoscientists from the US Geological Survey (USGS), California Geological Survey, Southern California Earthquake Center, and San Luis Obispo County.

10.0 References

Blanck, L. (2004a). San Simeon 6.5 magnitude earthquake, December 22, 2003: AEG News, Association of Engineering Geologists, V. 47, no. 1, p. 19.

Blanck, L. (2004b). Sympathetic moment for the 22 December 2003 San Simeon earthquake (abstr.): *Seismological Research Letters*, v. 74, No. 2, p. 294.

Boore, D., Joyner,W., and Fumal, T. (1997) Equations for estimating horizontal response spectra and peak acceleration from western North American earthquakes: A summary of recent work, *Seism. Res. Ltrs*, 68, p. 128-153. et al, 1997

Dehlinger, P., and B. A. Bolt (1987). Earthquakes and associated tectonics in a part of coastal central California, *Bull Seism. Soc. Am.* 77, 2056-2073.

Dreger, D. and P. Lombard (2004). Finite Source models of the 22 December 2003 San Simeon earthquake and applications to ShakeMap (abstr), *Seismological Research Letters*, v. 74, No. 2, p. 293.

Gomberg , J., Shedlock, K., and S. Roecker (1990). The effect of S-wave arrival times on the accuracy of hypocenter estimation, *Bull Seism. Soc. Am.* 80, 1605-1628.

Hall, C.A. (1974) Geologic map of the Cambria region, San Luis Obispo County, California: *U.S. Geological Survey Miscellaneous Field Studies Map MF-599*, 1:24,000 scale.

Hall, C.A. (1976) Geologic map of the San Simeon-Piedras Blancas region, San Luis Obispo County, California: *U.S. Geological Survey Miscellaneous Field Studies Map MF-784*, 1:24,000 scale.

Hardebeck, J.L., Boatwright, J., Dreger, D, Goel, R., Graizer, V., Hudnut, K., Ji, C., Jones, L., Langbine, J., Lin, J., Roeloffs, E., Simpson, R., Stark, K., Stein., R., and Tinsley, J.C. (2004). Preliminary report on the 22 December 2003, M 6.5 San Simeon, California, earthquake: *Seismological Research Letters*, V. 75, n. 2, pp. 155-172.

Ichinose G. and P. and Somerville (2004). Source depth and rupture process of the 2003 San Simeon earthquake from teleseismic data, preliminary report prepared for PG&E Geosciences.

Jennings, C. W. (1994). Fault activity map of California with locations and ages of recent volcanic eruptions: California Division of Mines and Geology, Geologic Data Map No 6, 1:750,000 scale.

Jennings, C.W. (1958). Geologic map of California, San Luis Obispo sheet: California Department of Natural Resources, Division of Mines, 1/250,000 scale.

Ji, C. and Tan, Y. (2004). Slip distribution of the 2003 San Simeon earthquake: an update (abstr.) *Seismological Research Letters*, v. 74, No. 2, p. 265.

Lettis, W.R., Hanson. L.L., Unruh, J.R., McLaren, M., and Savage, W.U., in press, Quaternary tectonic setting of south-central coastal California:

Lettis, W.R. and Hanson, K.L. (2004). The San Gregorio/Hosgri fault system, California: an evaluation of the style and rate of Quaternary deformation (abstr.): *Seismological Research Letters*, v. 74, No. 2, p. 264.

Klein, F. W. (1989). Users guide to HYPOINVERSE, a program for VAX computers to solve for earthquake locations and magnitudes, *U.S. Geol. Surv. Open file Rept. 89-314.*

McLaren, M. K. and W. U. Savage (2001). Seismicity of south-central coastal California: October 1987 though January 1997, *Bull Seism. Soc. Am.* 91, 1629-1658.

McLaren , M. K. and M. Stanton (2004). Comparison of the MW 6.5 San Simeon, California earthquake of 22 December 2003 and early aftershocks to 1987-1997 seismicity in the region (abstr.): *Seismological Research Letters*, v. 74, No. 2, p. 264.

Namson, J.S., and Davis, T.L. (2004). Tectonic model for the 22 December 2003 San Simeon earthquake (abstr.): *Seismological Research Letters*, v. 74, No. 2, p. 295.

Nuclear Regulatory Commission (NRC) (2004). Email from Girija Shukla (NRC) to Stan Ketelsen (PG&E), Subject: Re: Seismic phone call today at 1:00 PM EDT, 4/20/2004.

Pacific Gas and Electric Company (1988). Final report of the Diablo Canyon long-term seismic program, U.S. Nuclear Regulatory Commission docket Nos. 50-275 and 50-23.

Pacific Gas and Electric Company (1989). Response to question 43k regarding regional geologic cross sections, Diablo Canyon long term seismic program, U.S. Nuclear Regulatory Commission docket Nos. 50-275 and 50-323.

Reasenberg, P.A. and D. Oppenheimer (1985). FPFIT, FPPLOT, and FPPAGE: Fortran computer programs for calculating and displaying earthquake fault plane solutions, *U.S. Geol. Surv. Open File Rept. 85-739*.

Sadigh, K., Chang, C.Y., Egan, J.A., Makdisi, F., and Youngs, R.R. (1997). Attenuation relationships for shallow crustal earthquakes based on California strong motion data, *Seism. Res. Let.*, 68, p. 180-189.

Savage, W. U. and K. C. and McNally (1974). Moderate earthquake seismicity in central California: 1936-1973, in Program for the 70th Annual meeting of the Seismological Society of America.

Toppozada, T. D., C. R. Real, and D. L. Parke (1981). Preparation of isoseismal maps and summary of reported effects for pre-1900 California earthquakes, 1800-1999. *Calif. Div. Mines and Geol. Open File Rept. 81-11, SAC*, 182 pp.

Treiman, J.A., Tinsley, J.C., Rosenberg, L.I., Keefer, D.K., Knudson, K.L., Lloyd, R.C., Manson, M.W., McCrink, T.P., Reid, M.E., Schmidt, K., and Wilson, R.I. (2004) Surface effects of the 22 December 2003 Mw 6.5 San Simeon earthquake (abstr.): *Seismological Research Letters*, v. 74, No. 2, p. 264.

U.S. Geological Survey (USGS) (2004). Northern California Seismic Network. On-line at http://quake.geo.berkeley.edu/ncedc/catalog-search.html, accessed 5/12/04.

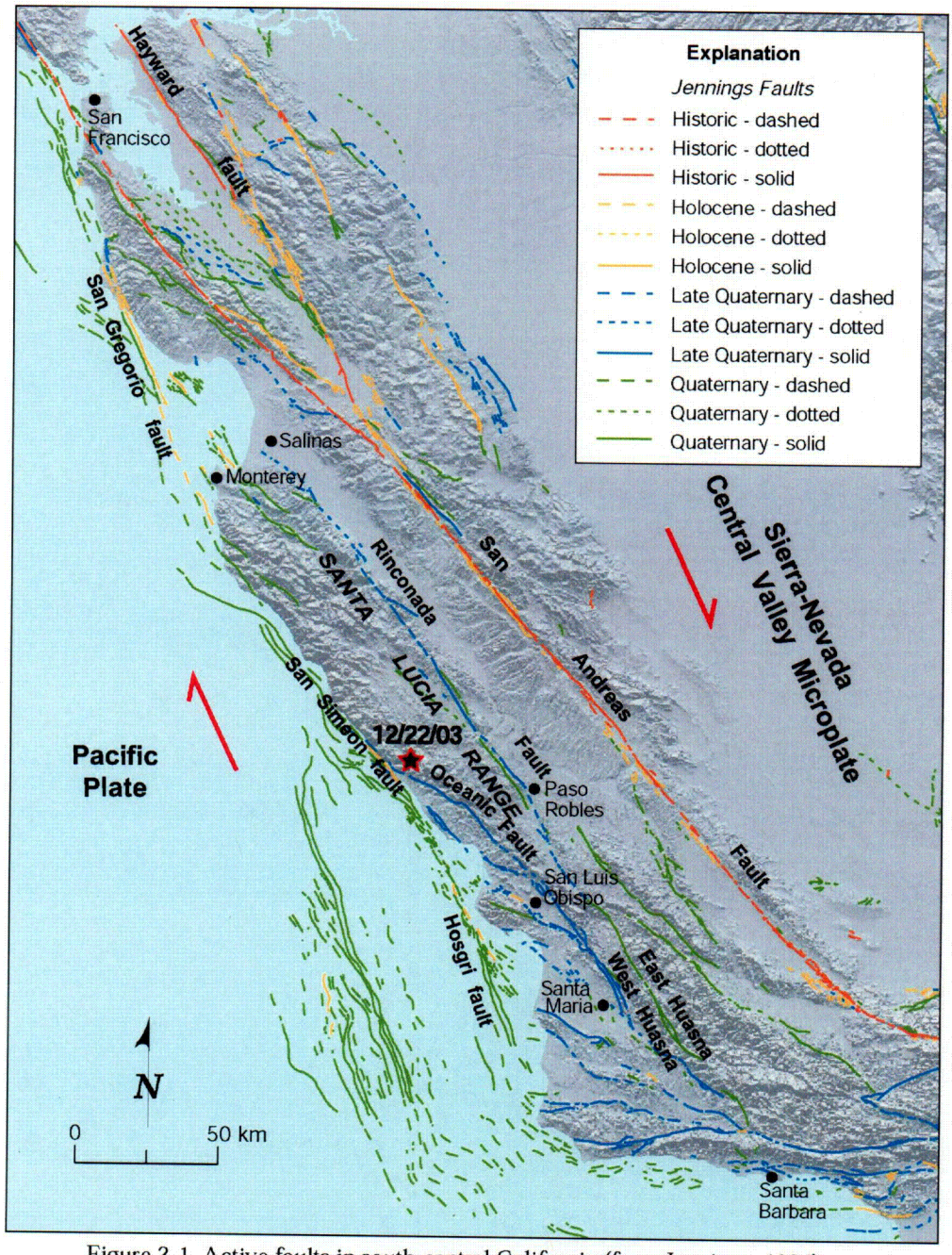

Figure 2-1. Active faults in south-central California (from Jennings, 1994).

C01

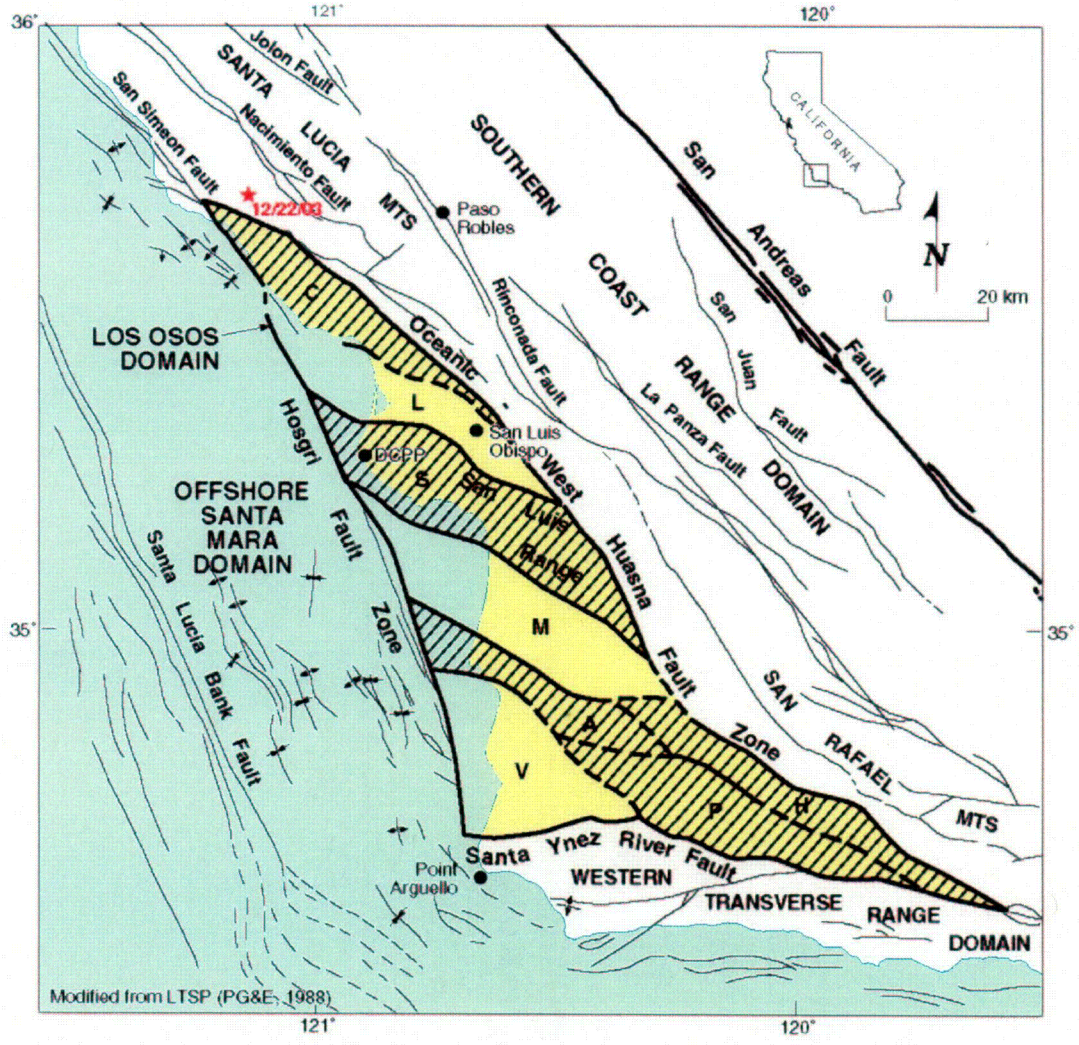

Figure 2-2. Major kinematic domains in western central California, including the Los Osos domain, offshore Santa Maria basin domain, Southern Coast Ranges domain (including the Santa Lucia and San Rafael Mountains) and western Transverse Ranges domain. The Los Osos domain is divided into distinct structural blocks including: C-Cambria, L-Los Osos Valley, S-San Luis/Pismo, M-Santa Maria Valley, A-Casmalia, H-Solomon Hills, V-Vandenberg/Lompoc, P-Purisima. Hachured areas show location of Quaternary uplift within the Los Osos domain. Bedrock and Quaternary faults shown as light lines; domain boundary faults shown as bold lines. DCPP - Diablo Canyon power plant.

C02

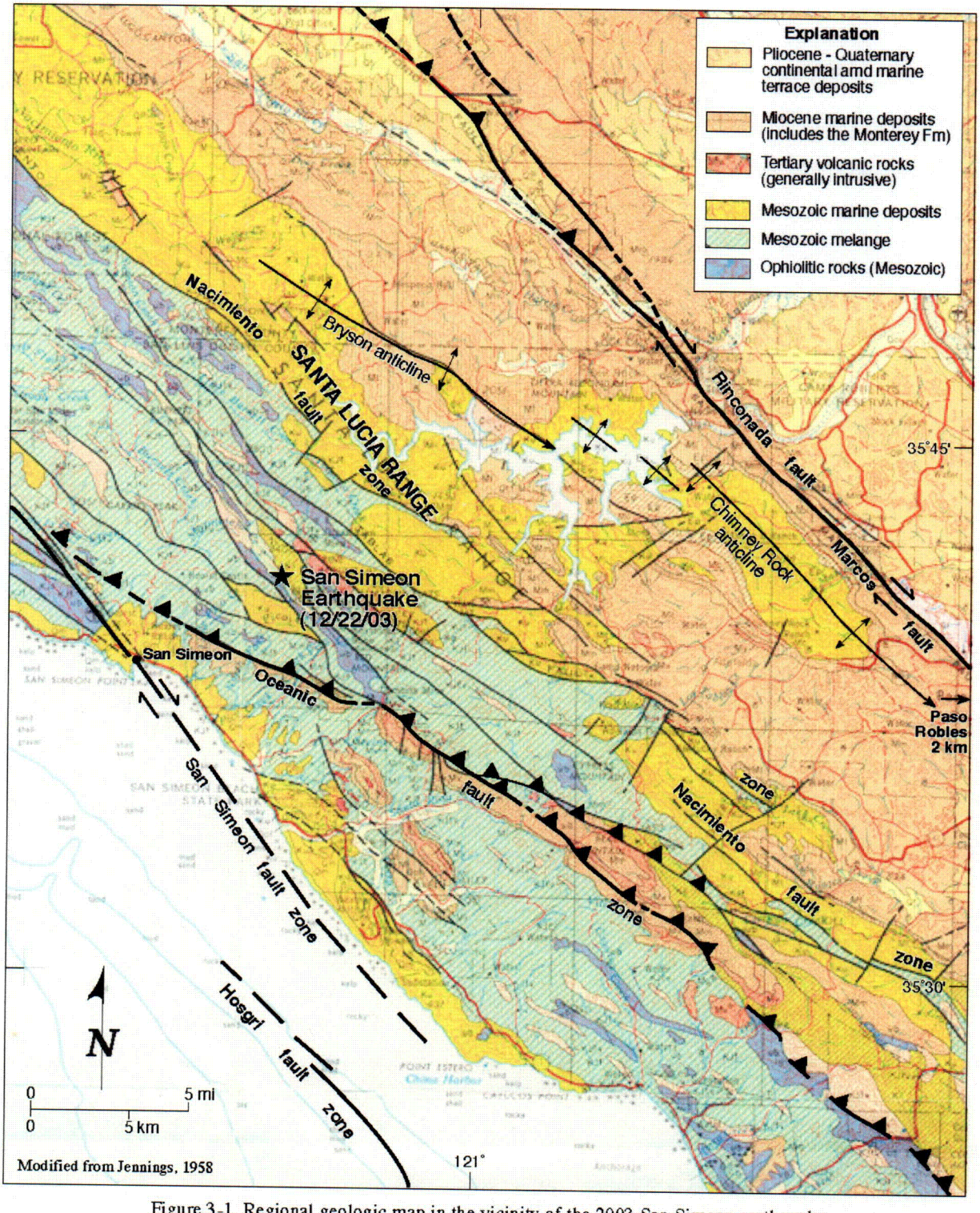

Figure 3-1. Regional geologic map in the vicinity of the 2003 San Simeon earthquake.

C03

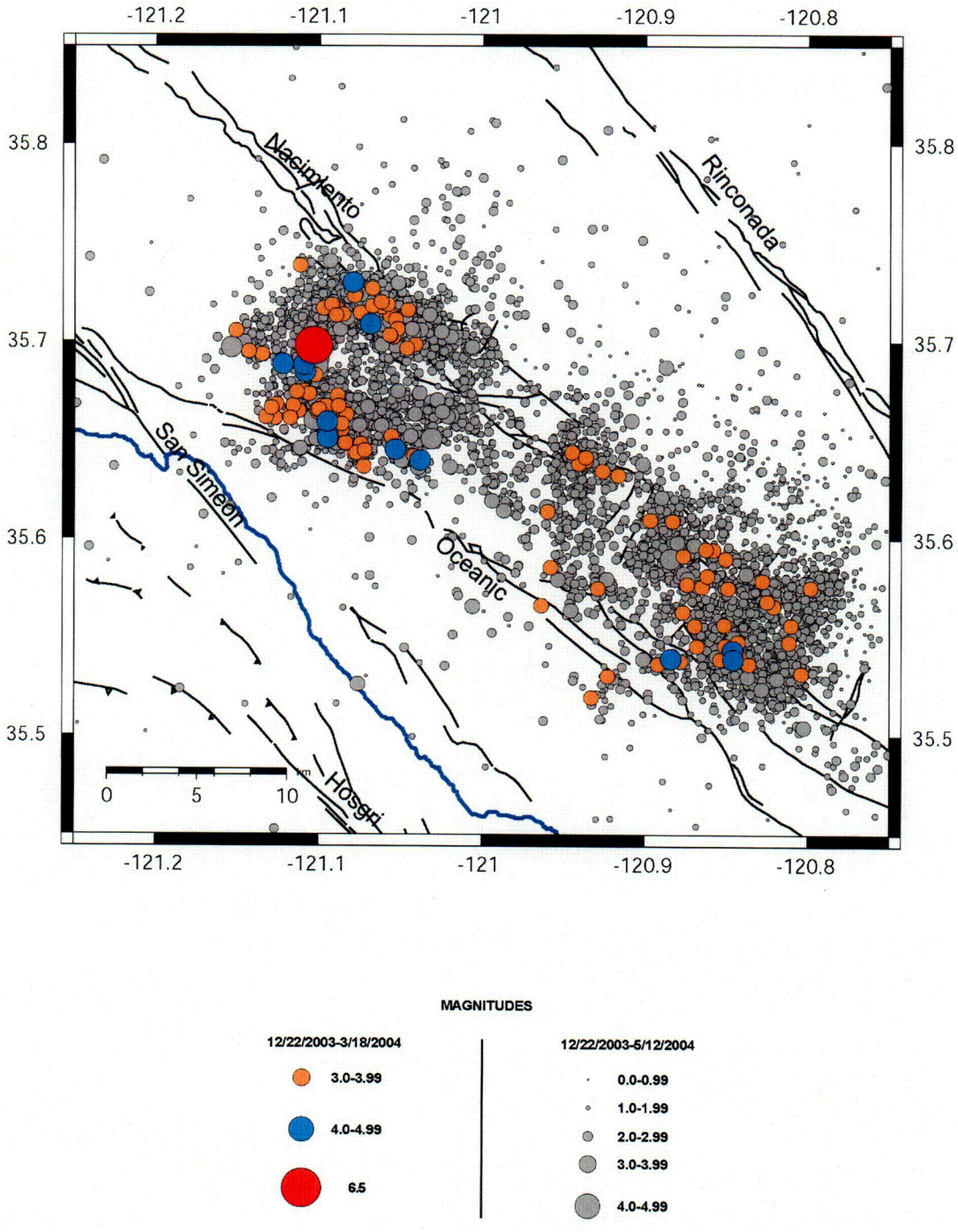

Figure 5-1. Map of San Simeon aftershocks from 22 December 2003 to 12 May 2004 (gray circles) from the USGS Northern California Data Center online database (USGS, 2004) and the San Simeon main shock and M3 and greater aftershocks relocated using PG&E and USGS arrival time data.

C04

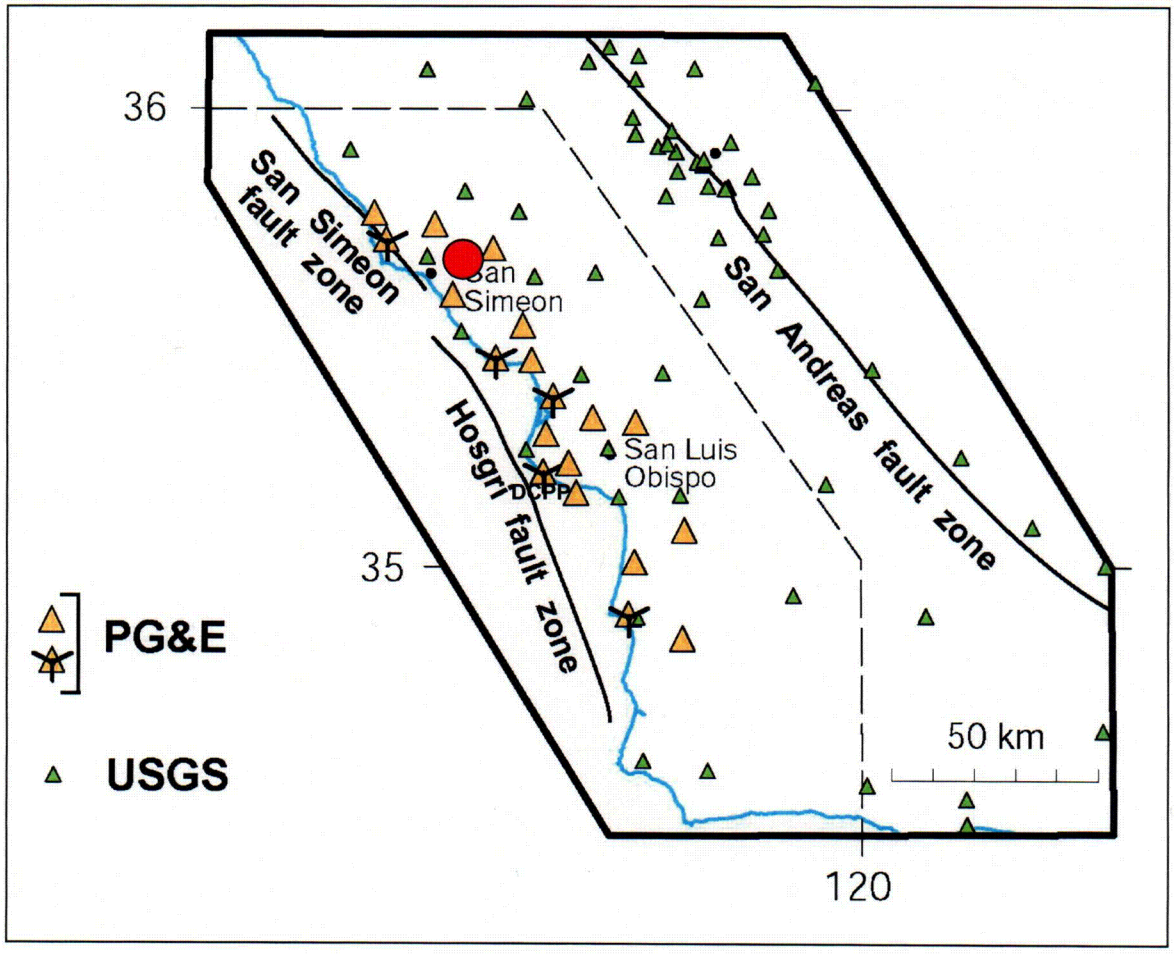

Figure 5-2. Map showing PG&E (yellow triangles) and USGS (green triangles) seismographic stations. The PG&E stations with three tic marks are 3-component, dual gain instruments. The main shock location (large red circle) is also shown. Primary offshore faults are labeled. Dashed line marks the PG&E study area from McLaren and Savage (2001).

C05

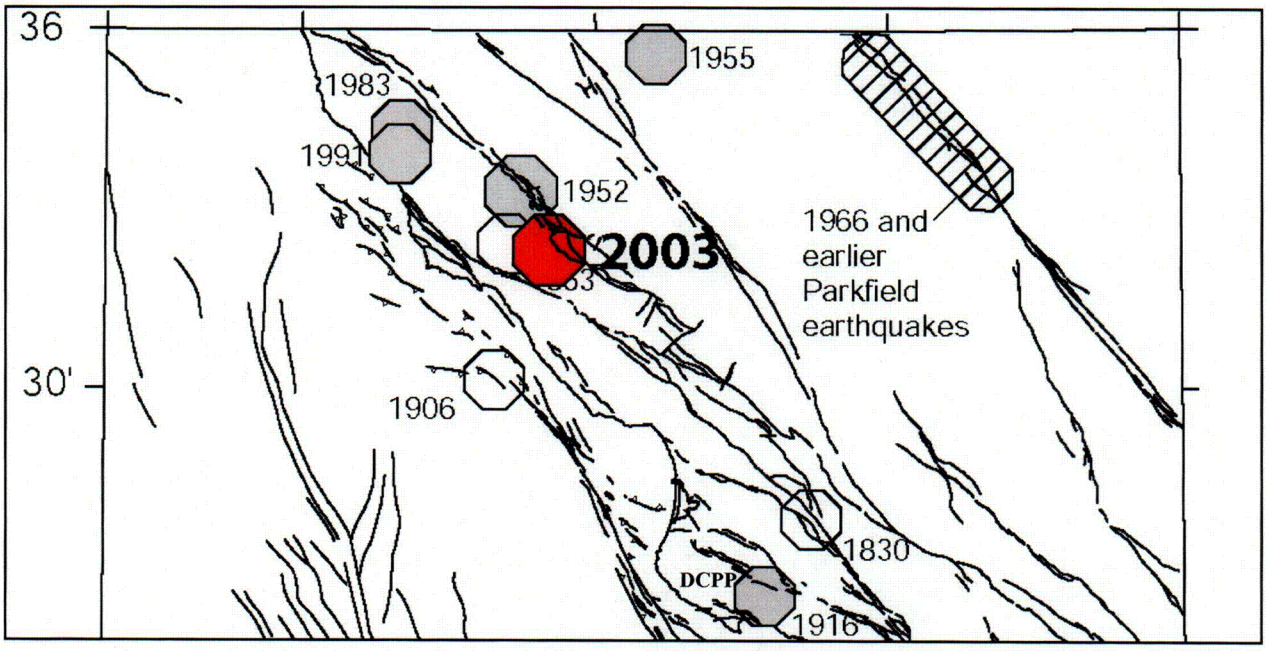

Figure 5-3. Historic seismicity; M5 and greater earthquakes since 1830 (McLaren and Savage, 2001). Red circle is the 22 December 2003 main shock.

C06

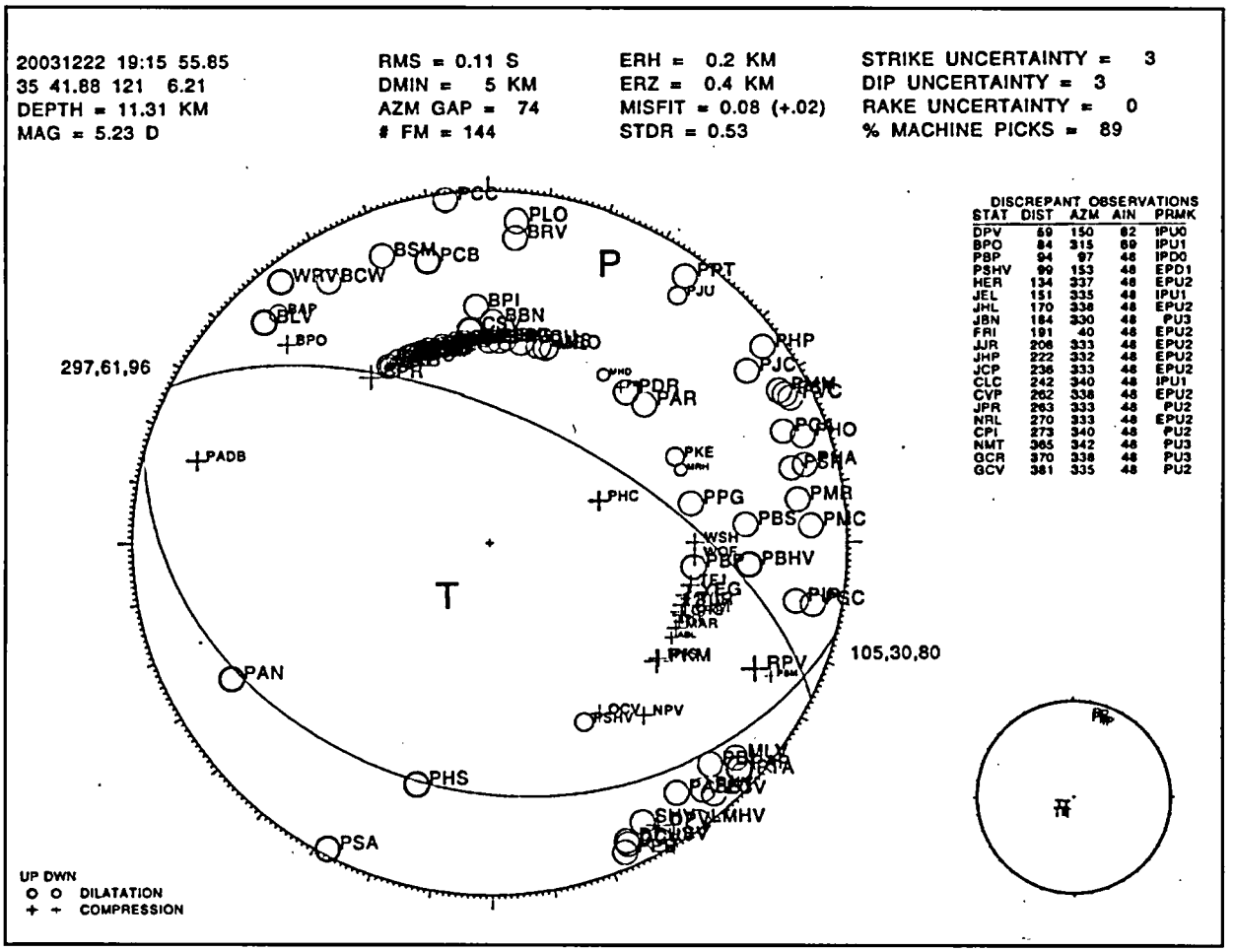

Figure 5-4. Focal mechanism of the 22 December 2003 San Simeon main shock.

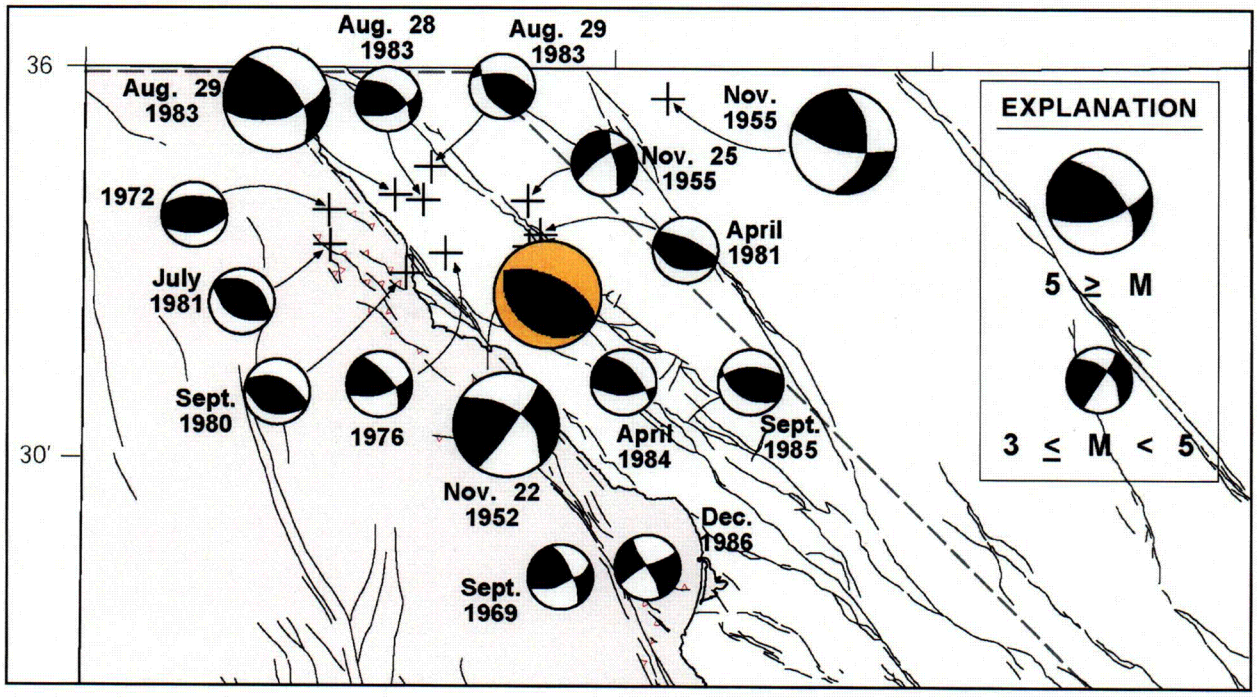

Figure 5-5. Comparison of focal mechanisms of M3 and greater events in the San Simeon region (McLaren and Savage , 2001) with the 22 December 2003 main shock mechanism. The 22 November 1952 Bryson earthquake mechanism is located beneath the main shock.

C07

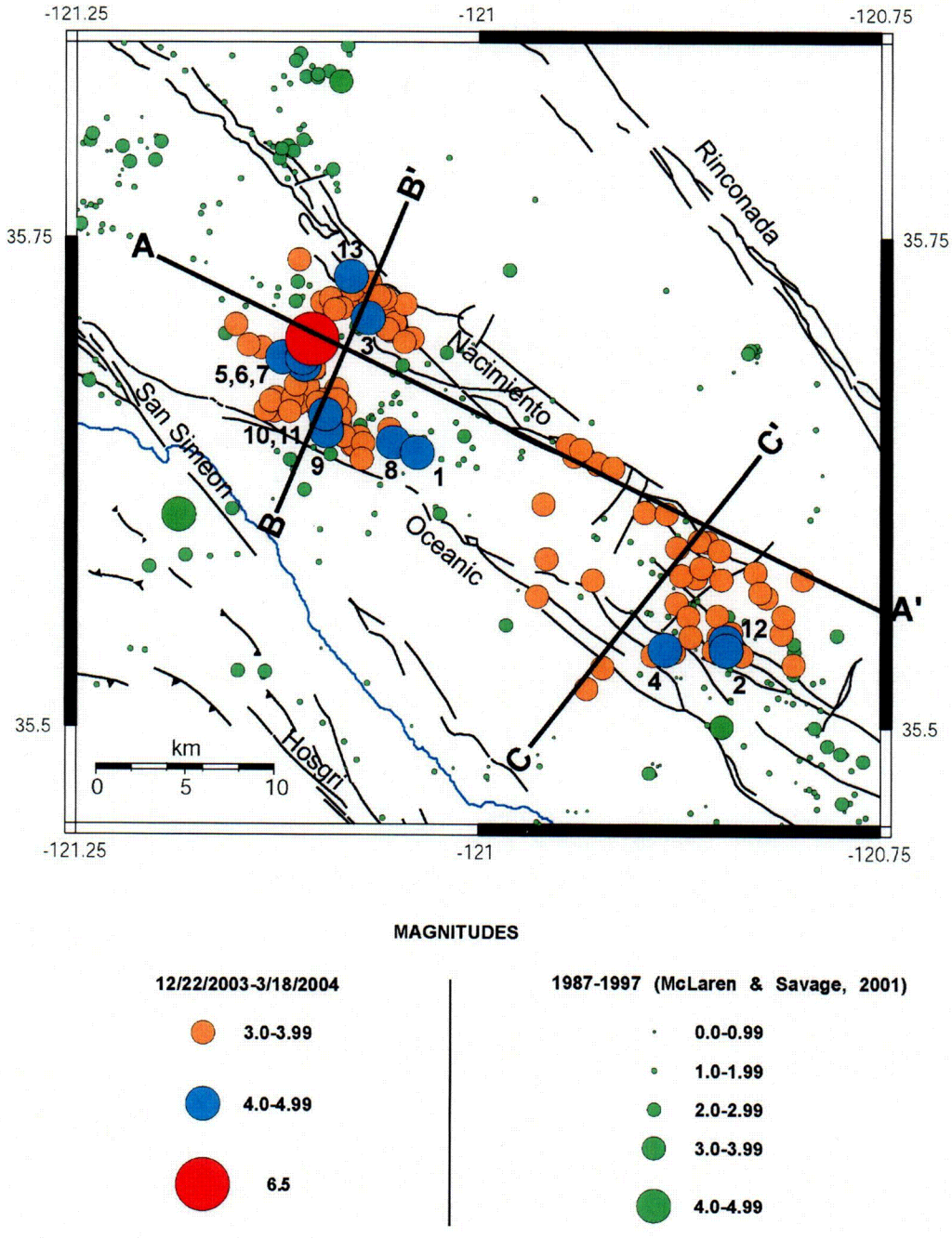

Figure 5-6. Map of the San Simeon main shock, aftershocks and previous seismicity from McLaren and Savage (2001). Faults are from PG&E (1988). Seismic cross sections A through C are also shown (Fig. 5-6). M4 aftershocks are numbered according to order of occurrence (see Section 5.3 for discussion).

C08

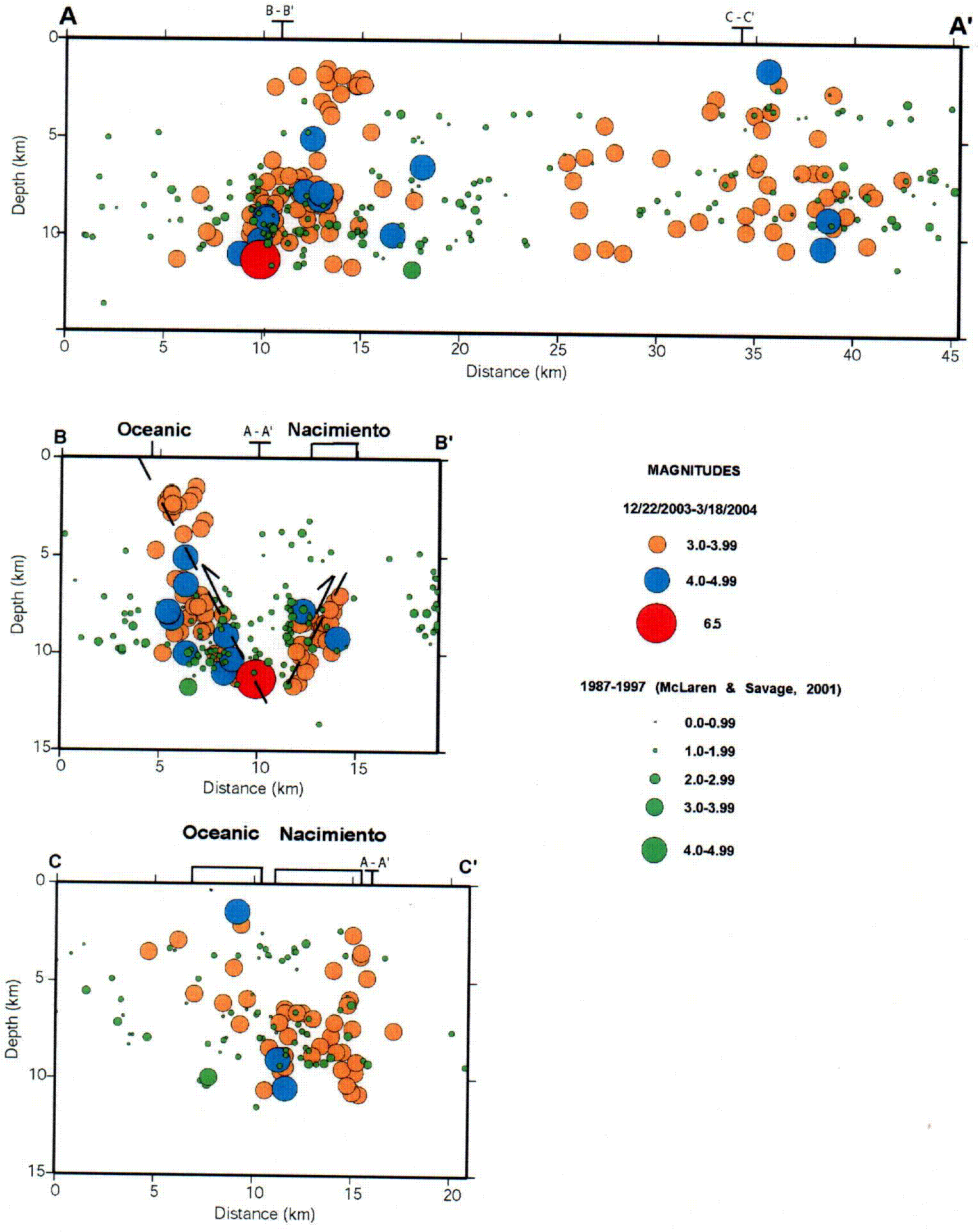

Figure 5-7. Seismic cross sections A through C showing the San Simeon main shock, aftershocks and previous seismicity from McLaren and Savage (2001). Earthquakes are projected within 8 km onto cross section AA' and 10 km onto sections BB' and CC'. See Figure 5-2 for locations of cross sections. The surface locations of the Oceanic and Nacimiento faults are projected on to the cross sections. Cross section intersection points are also marked. Possible fault planes with hanging wall fault motions are shown in cross section BB' near the main shock and NE of the main shock (dashed lines).

C09

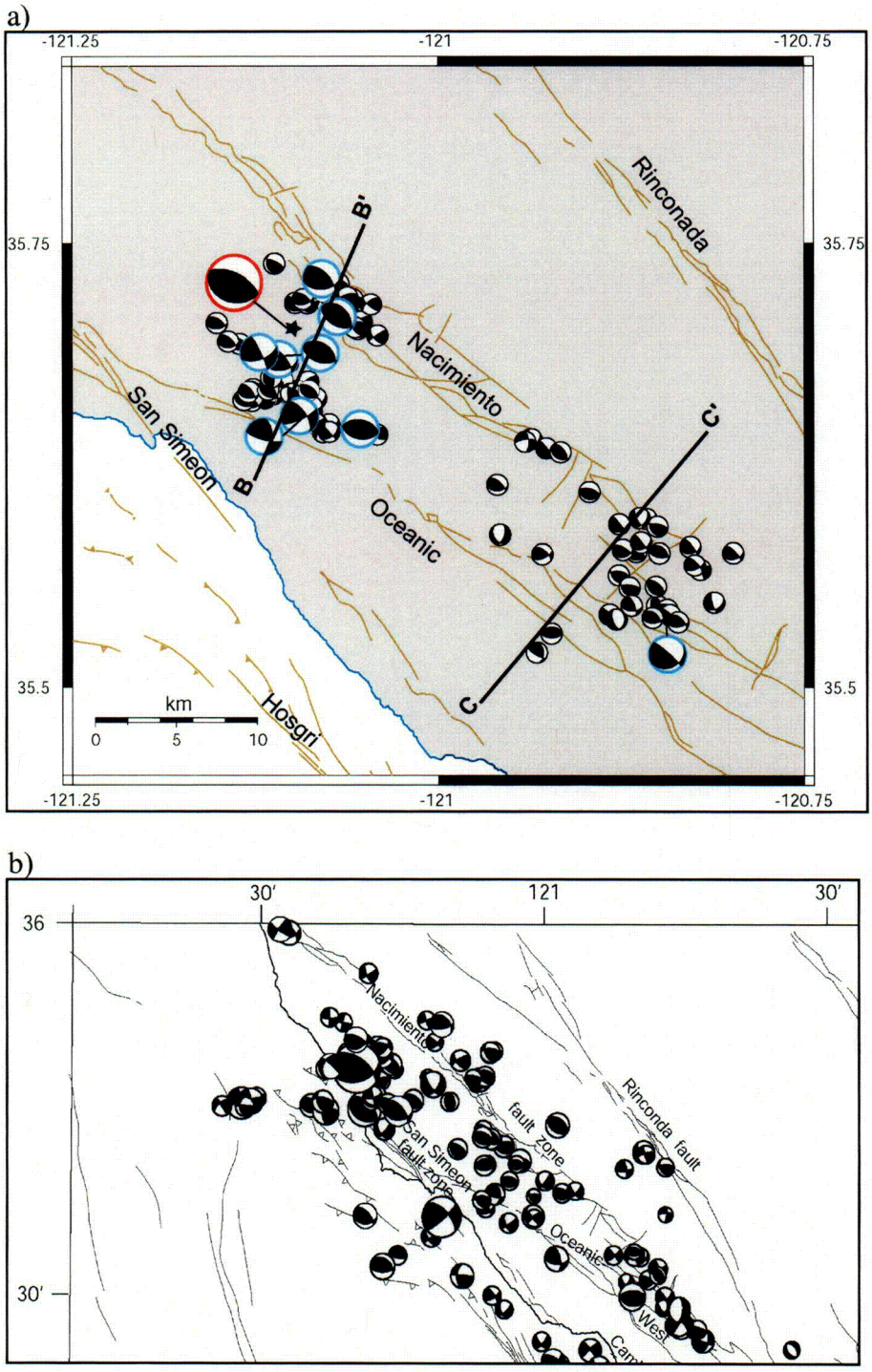

Figure 5-8. a) Map of lower hemisphere P-wave first motion focal mechanisms for the main shock (red outline) and aftershocks (blue outlines are M4 events) with locations of focal mechanism cross sections (Fig. 5.8); b) Focal mechanisms of 1987-1997 events from McLaren and Savage (2001).

C10

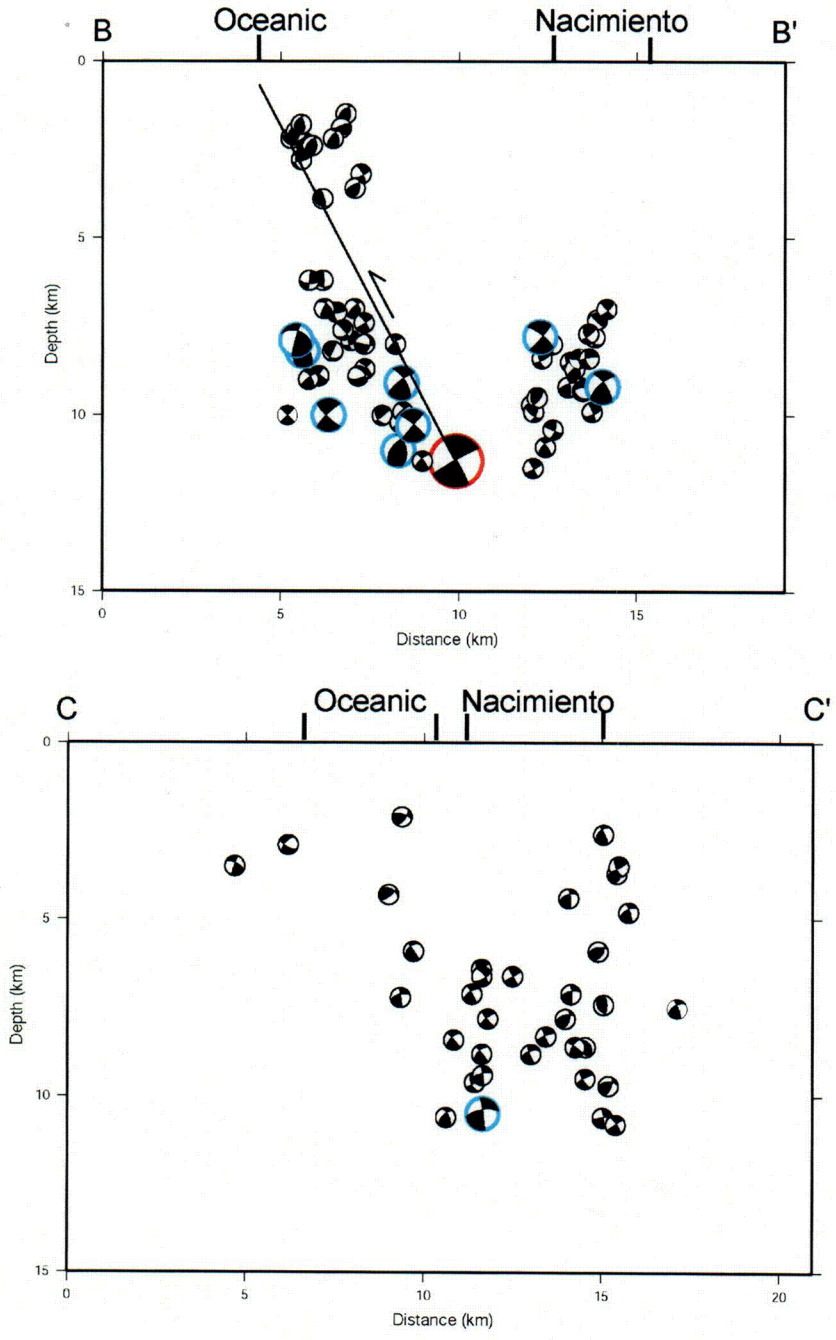

Figure 5-9. Lower hemisphere P-wave first motion focal mechanisms for the main shock (red outline) and aftershocks (blue outlines are M4 events) projected on to cross sections BB' and CC'; locations correspond to the seismic cross sections of Fig. 5.5. The surface locations of the Oceanic and Nacimiento faults are projected on to the cross sections. The preferred fault plane of the main shock is shown on cross section BB' with the hanging wall sense of motion (solid line).

C11

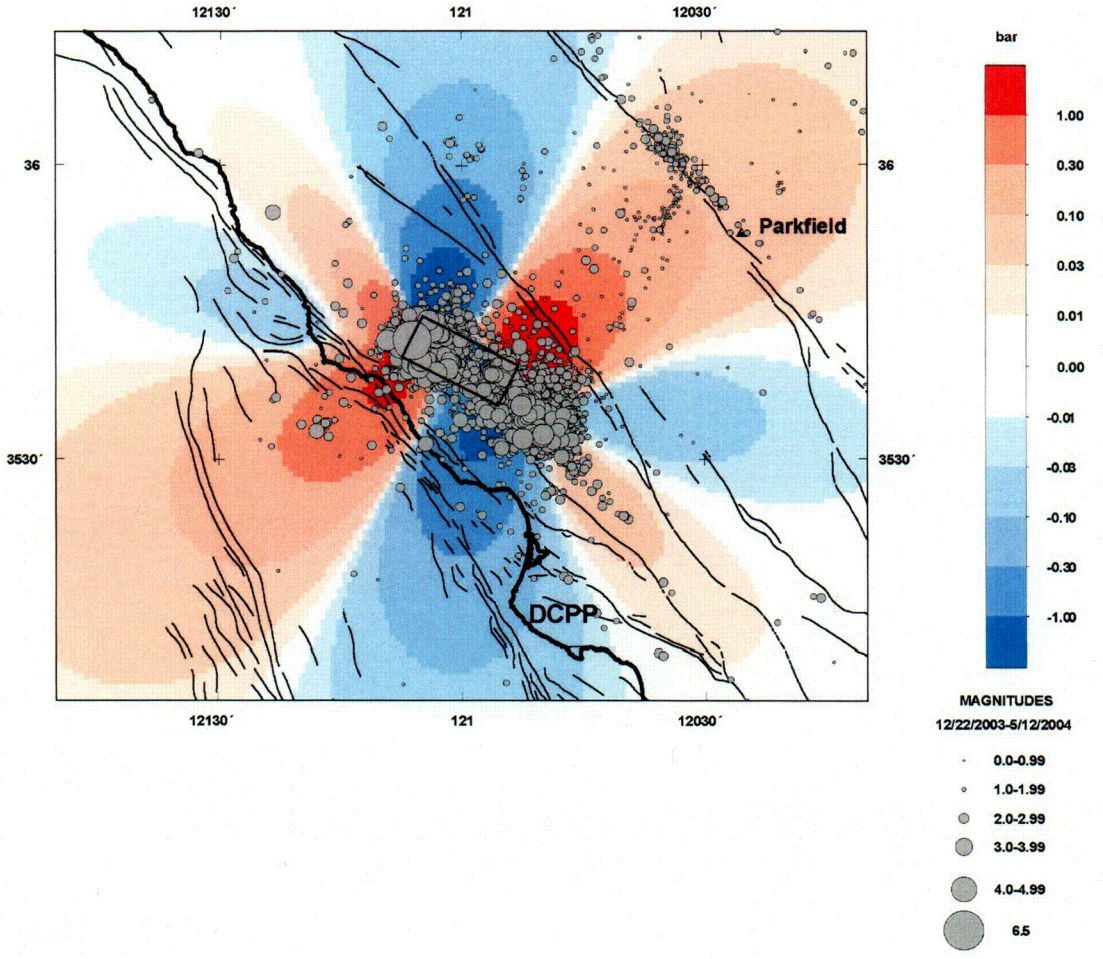

Figure 5-10. Comparison of regional static stress changes due to the San Simeon earthquake and aftershock activity. Coulomb stress changes on planes striking parallel to the San Andreas fault (N 40 W, dip 90, rake 180) in the vicinity of Parkfield are shown for cases where right-lateral strike slip faulting is encouraged (red) or discouraged (blue) (from Hardebeck et al., 2004). Non-San Simeon aftershock seismicity during the period Dec 22, 2003 to May 12, 2004 appears to be preferentially clustered in the area between the Rinconada and San Andreas faults near Parkfield, as well as offshore near the San Simeon fault.

C12

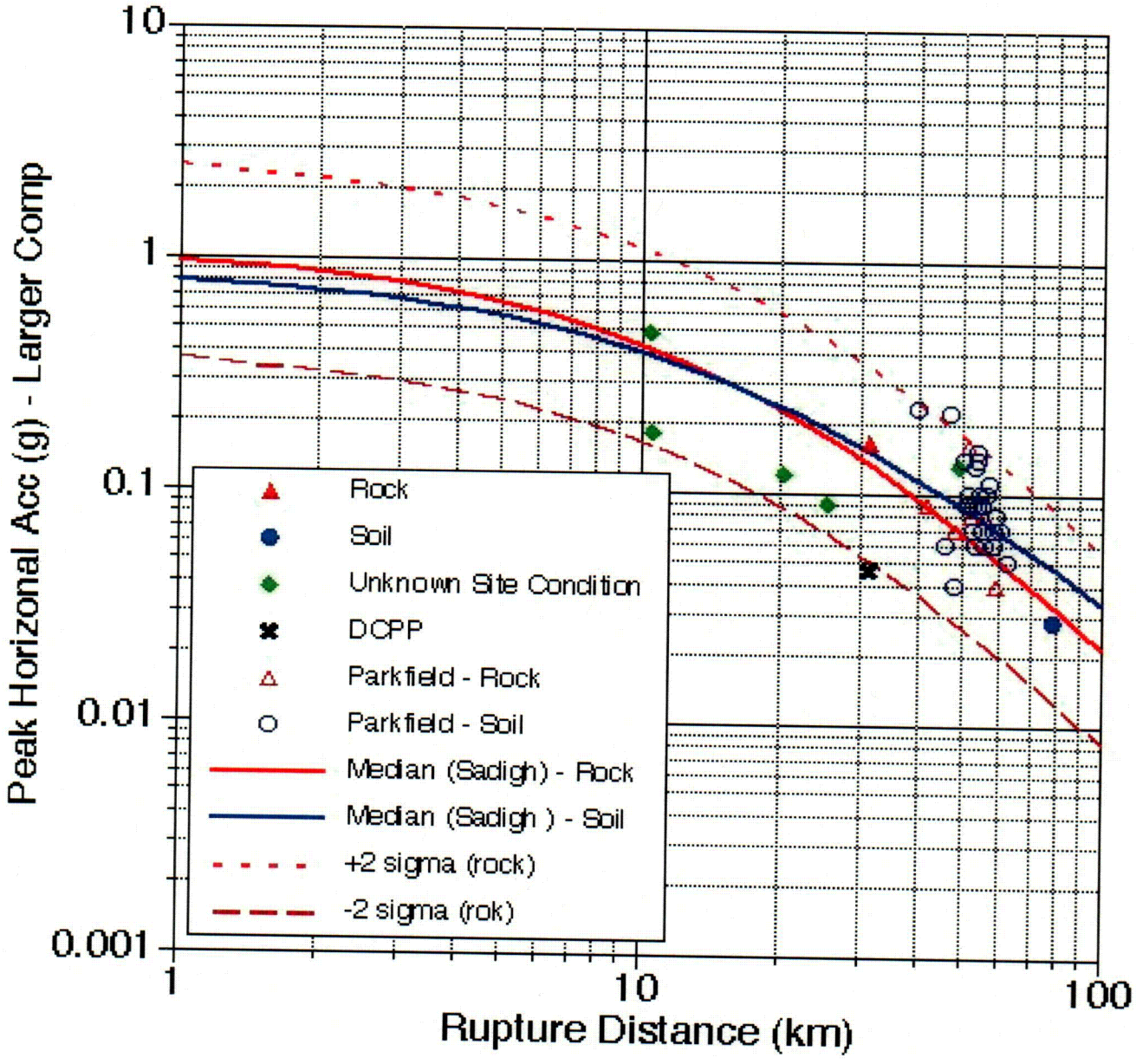

Figure 6-1. Attentuation of peak horizontal acceleration from the San Simeon earthquake mainshock

C13

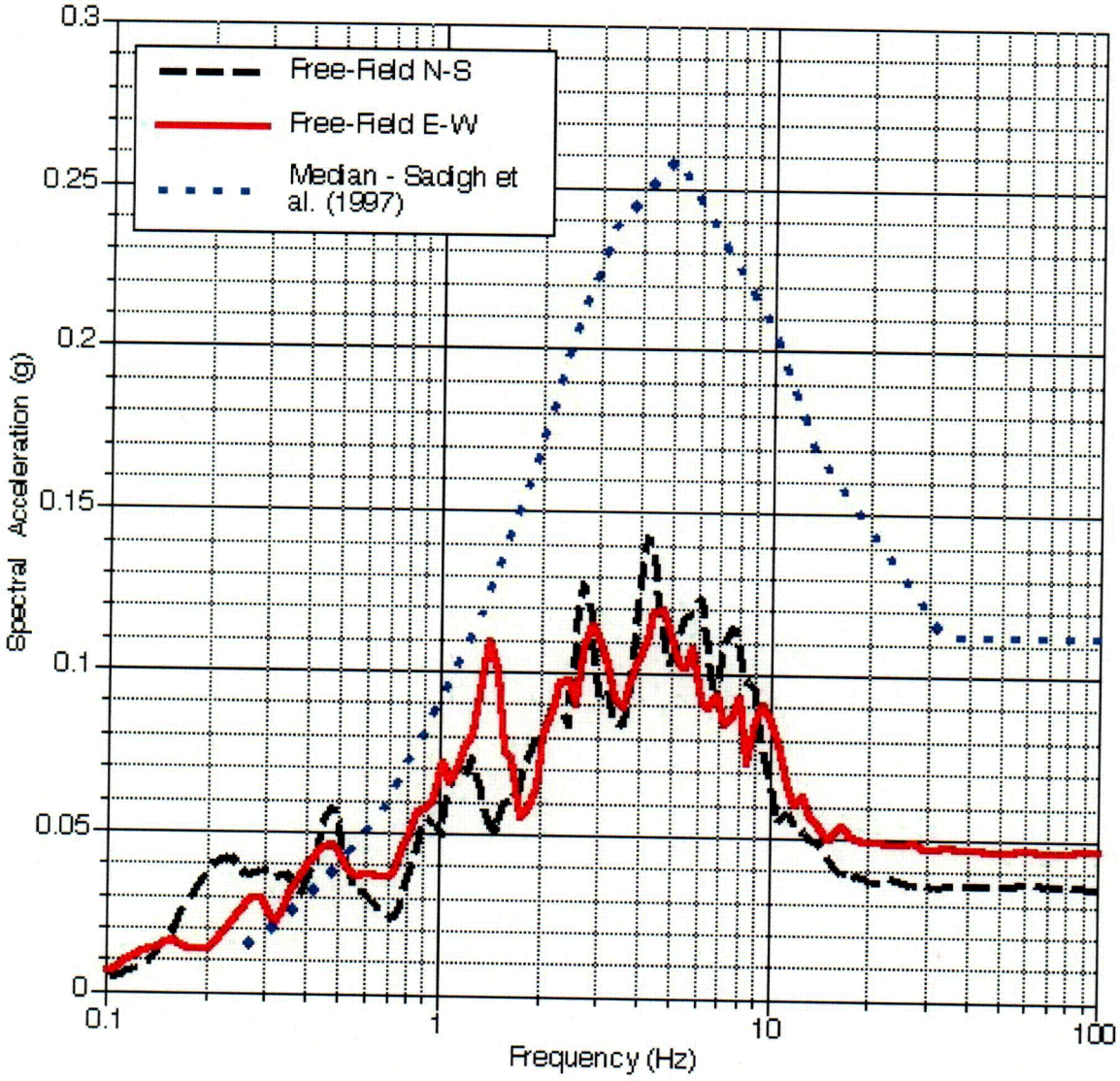

Figure 6-2 Free field spectral values recorded at the plant site compared to Sadigh et al (1997) median spectrum.

C14

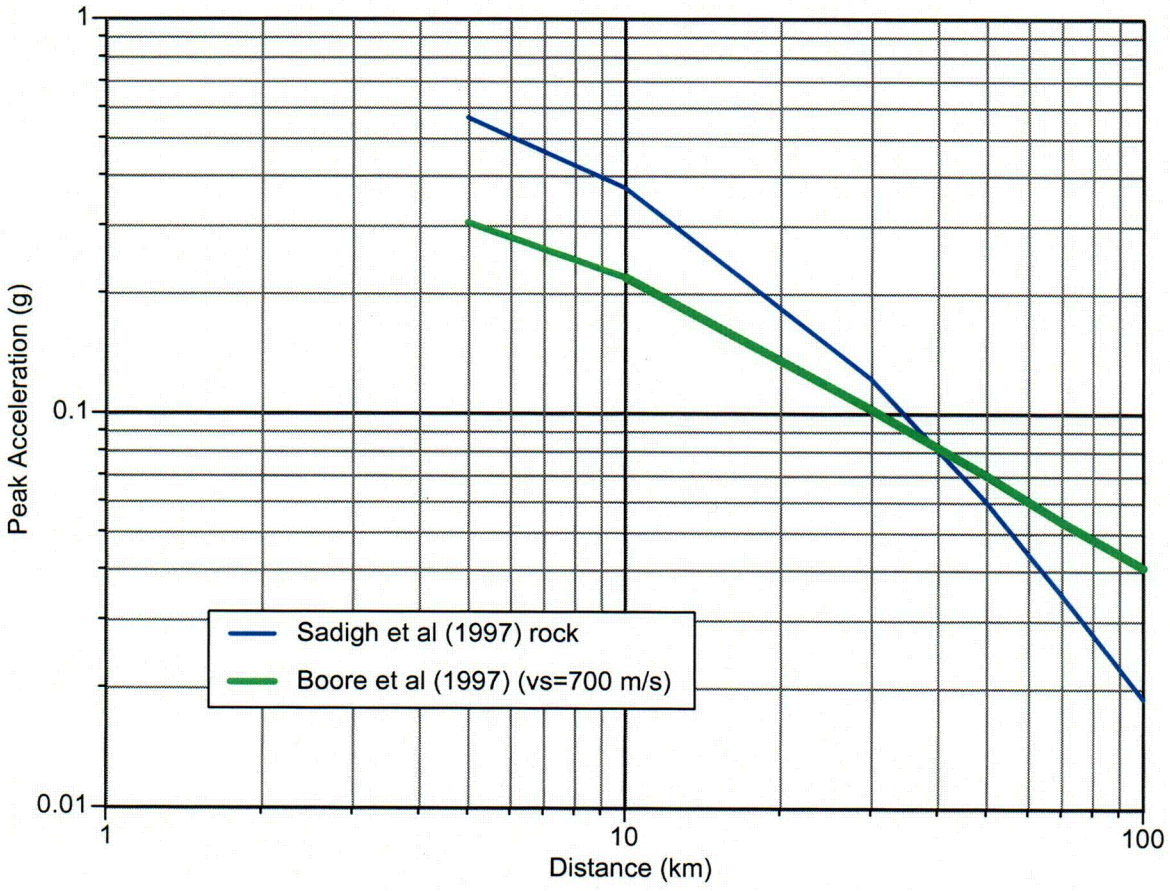

Figure 6-3. Comparison of the Sadigh et al (1997) attenuation relation to Boore et al (1997).

C15

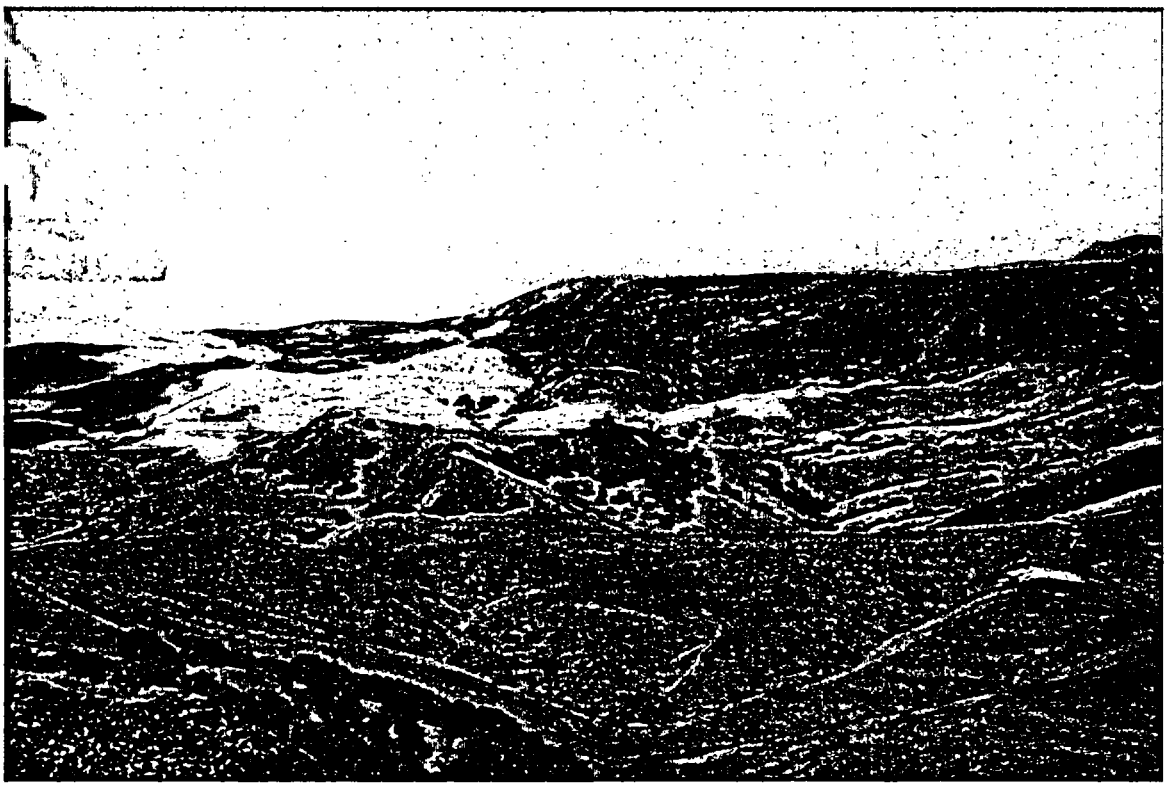

Photo 1. Western range front of the Santa Lucia Range north of San Luis Obispo. View looking northwest with the Oceanic fault in the middle right of the photo. (Photo #CluffLO-R3-008-2A, 1/15/04)

Photo 2. Foothills of the western range front of the Santa Lucia Range between San Luis Obispo and San Simeon. View looking east; the Oceanic fault lies in the distance between the distant ridge and the hills in the middle of the photo (Photo #CluffLO-R1-014-5A, 1/15/04).

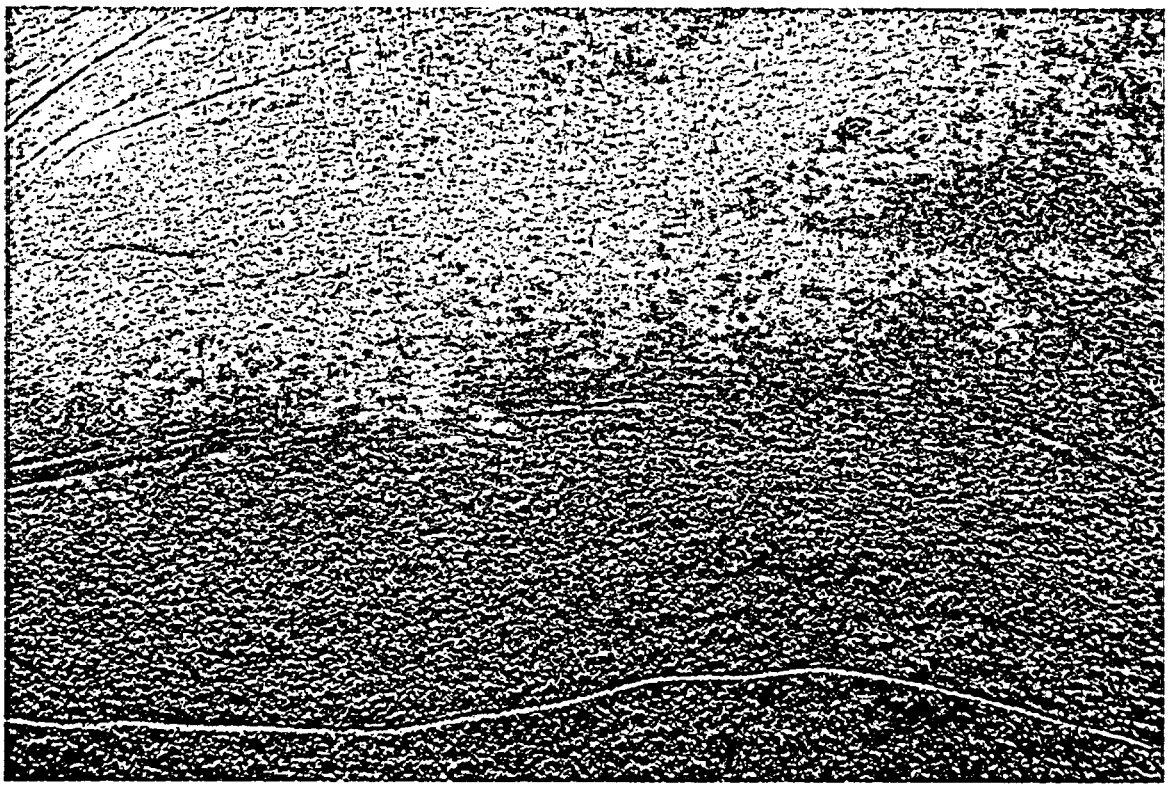

Photo 3. Typical scarplett at the head of an incipient landslide along Santa Lucia Range front. Scarplet is in middle and middle left and is clearly visible and significantly smaller than the cow trail that traverses the lower part of the photo. (Photo #CluffLO-R1-010-3A, 1/15/04).

Photo 4. Typical ground crack and scarp at head of pre-existing, dormant landslide at the Gates Ranch, Shadow Canyon Road, Templeton. (Photo courtesy of Lew Rosenberg, Geologist, San Luis Obispo County)

Photo 5. Scarps on the sackungen at the Hartzel Ranch in the Santa Lucia Range. View to the north; bedrock is serpentine. (Photo courtesy of John Tinsley, Geologist, US Geological Survey)

Table 5-1
Location parameters of the San Simeon earthquake and magnitude 3 and greater aftershocks, 22 December 2003 to 18 March 2004

Cluster	Date	Time (UTC)		Latitude (N)	Longitude (W)		Depth	Mag.**	Number P&S-wave readings	Number S-wave readings	Azm. gap	Closest Station	Closest Station with S-wave reading	RMS	Horiz. Error	Vert. Error
	YYYYMM DD	hr:min	sec.	deg. min.	deg. min.		(km)	ML			(deg)	(km)	(km)	(sec)	(km)	(km)
SW	20031222	19:15	55.85	35 41.88	121	6.21	11.3	6.5 M_W	79	1	74	5.0	10.9	0.11	.19	.36
SW	20031222	19:26	6.86	35 38.40	121	2.3	6.5	4.73 (1)	27	4	102	14.0	20.4	0.14	.45	1.58
SE	20031222	19:31	4.95	35 32.35	120	50.75	9.0	4.02 (2)	17	2	86	15.0	14.7	0.08	.61	2.28
SE	20031222	19:35	28.23	35 33.79	120	52.61	6.5	3.3	61	5	37	4.0	14.4	0.15	.22	.75
SE	20031222	19:37	43.68	35 35.15	120	57.47	4.3	3.6	31	4	64	12.0	13.7	0.12	.28	2.98
SE	20031222	19:41	4.90	35 32.77	120	51.03	6.6	3.4	41	3	74	15.0	18.5	0.07	.36	1.59
SE	20031222	19:46	38.61	35 35.68	120	51.47	3.7	3.4	64	3	72	18.0	18.2	0.11	.20	1.61
NE	20031222	21:31	36.12	35 42.54	121	4.13	7.8	4.33 (3)	81	3	58	8.0	18.3	0.11	.18	.50
SE	20031222	21:37	15.78	35 33.99	120	57.81	5.7	3.3	74	4	52	6.0	11.5	0.11	.18	.57
SE	20031222	22:39	17.49	35 33.38	120	52.17	9.6	3.2	59	3	60	11.0	14.3	0.09	.20	.77
NE	20031222	23:35	54.96	35 42.83	121	5.12	10.1	3.8	60	5	57	7.0	12.1	0.11	.22	.61
SE	20031222	23:52	36.26	35 32.37	120	53.03	1.4	4.1 (4)	61	3	45	2.0	12.1	0.09	.16	.69
SE	20031223	0:05	59.02	35 32.46	120	52.98	7.3	3.6	56	4	45	9.0	12.2	0.08	.19	.56
SE	20031223	1:18	4.61	35 34.74	120	49.67	4.8	3.4	55	3	49	8.0	18.7	0.14	.21	.90
SW	20031223	2:06	55.00	35 41.09	121	6.52	9.1	4.23 (5)	75	4	95	4.0	15.0	0.11	.19	.42
SE	20031223	2:35	8.57	35 32.63	120	50.62	7.8	3.0	60	3	33	6.0	15.3	0.09	.19	.73
SW	20031223	3:46	0.56	35 41.32	121	7.34	11.0	4.3 (6)	57	3	91	3.0	15.0	0.11	.23	.37
SE	20031223	4:00	21.89	35 33.41	120	51.08	6.6	3.1	49	4	42	6.0	15.5	0.1	.19	.62
SE	20031223	5:00	55.83	35 31.55	120	49.61	8.6	3.5	46	1	53	7.0	15.4	0.1	.19	.63
NE	20031223	5:47	41.40	35 42.20	121	3.42	8.5	3.3	67	3	90	9.0	19.4	0.1	.18	.52
SE	20031223	8:03	34.01	35 36.55	120	52.99	9.1	3.5	66	3	30	4.0	18.4	0.09	.17	.42
SE	20031223	8:14	10.33	35 32.89	120	50.57	6.6	3.3	60	3	45	6.0	15.5	0.09	.20	.74
SE	20031223	10:15	6.05	35 35.70	120	51.75	9.7	3.0	57	3	56	8.0	18.0	0.08	.20	.96

Cluster	Date	Time (UTC)		Latitude (N)	Longitude (W)	Depth	Mag.**	Number P&S-wave readings	Number S-wave readings	Azm. gap	Closest Station	Closest Station with S-wave reading	RMS	Horiz. Error	Vert. Error
	YYYYMMDD	hr:min	sec.	deg. min.	deg. min.	(km)	ML			(deg)	(km)	(km)	(sec)	(km)	(km)
SE	20031223	10:47	31.15	35 34.50	120 55.73	5.9	3.4	60	3	81	5.0	13.2	0.1	.19	.63
SW	20031223	11:40	36.12	35 41.30	121 6.58	10.3	4.18 (7)	65	1	90	4.0	58.2	0.1	.20	.44
SW	20031223	11:53	37.04	35 39.67	121 5.11	1.6	3.4	54	2	101	7.0	17.7	0.11	.23	1.03
SE	20031223	12:07	31.28	35 35.42	120 51.01	3.5	3.3	60	3	53	6.0	18.3	0.1	.19	.94
SE	20031223	1707	5.04	35 38.39	120 56.19	5.9	3.0	61	3	34	6.0	20.0	0.09	.16	.58
SW	20031223	1817	10.87	35 38.72	121 3.2	10.0	4.6 (8)	54	0	73	6.0	51.8	0.08	.21	.47
SW	20031223	1931	4.59	35 40.04	121 5.91	7.9	3.4	60	4	119	16.0	16.3	0.1	.25	.74
SE	20031223	2017	12.53	35 32.30	120 52.7	2.1	3.3	60	3	46	3.0	12.3	0.12	.18	.45
SE	20031223	2153	42.30	35 33.98	120 49.25	7.4	3.0	57	4	47	18.0	18.3	0.09	.18	1.03
SW	20031224	2:08	15.73	35 40.35	121 5.32	10.0	3.6	48	3	113	17.0	17.0	0.09	.22	.55
NE	20031224	2:36	11.99	35 42.13	121 3.29	11.5	3.6	55	3	75	12.0	19.6	0.12	.22	.50
SW	20031224	2:41	42.96	35 39.93	121 5.14	3.2	3.5	49	3	101	7.0	17.5	0.12	.24	1.09
SW	20031224	3:58	10.83	35 40.04	121 5.74	7.0	3.0	60	4	109	6.0	5.5	0.11	.21	.61
SW	20031224	5:22	28.37	35 40.50	121 6.58	8.7	3.7	69	5	112	4.0	15.1	0.12	.20	.49
SW	20031224	5:31	49.24	35 39.85	121 6.06	7.1	3.5	62	3	114	5.0	16.2	0.11	.19	.53
NE	20031224	5:52	8.31	35 42.79	121 3.41	8.5	3.4	60	3	73	13.0	19.4	0.11	.18	.64
SE	20031224	9:36	8.44	35 32.45	120 50.5	9.4	3.7	62	2	34	6.0	15.1	0.09	.18	.53
SE	20031224	14:32	51.52	35 31.83	120 55.36	2.9	3.5	63	4	82	1.0	9.0	0.1	.20	.44
SE	20031224	15:27	6.12	35 34.13	120 49.48	2.6	3.1	56	3	36	8.0	18.0	0.12	.19	1.21
SE	20031224	16:59	6.74	35 32.21	120 53.5	6.1	3.1	52	1	68	9.0	18.4	0.09	.22	.88
SW	20031224	20:14	19.90	35 39.78	121 5	3.6	3.5	70	5	99	7.0	17.8	0.11	.18	.84
SW	20031224	23:59	42.99	35 38.62	121 4.64	2.4	3.6	58	3	95	5.0	19.0	0.1	.16	.47
SW	20031225	0:20	0.83	35 38.91	121 5.03	1.9	3.2	15	1	102	5.0	22.7	0.07	.31	.90
SW	20031225	5:20	13.26	35 39.16	121 5.68	8.3	4.2 (9)	60	2	138	15.0	39.8	0.08	.23	.61
SW	20031225	5:21	59.07	35 39.06	121 5.69	7.9	4.3 (10)	34	4	124	6.0	17.2	0.1	.27	.83
SW	20031225	6:06	36.44	35 39.32	121 5.18	3.9	3.3	63	4	103	6.0	17.8	0.12	.21	.97
SW	20031225	6:37	44.86	35 38.54	121 2.51	8.2	3.1	42	4	127	11.0	20.7	0.09	.26	.84
SW	20031225	6:44	19.43	35 39.93	121 6.08	1.9	3.1	58	4	114	5.0	16.1	0.12	.19	.68

Cluster	Date	Time (UTC)		Latitude (N)	Longitude (W)		Depth	Mag.**	Number P&S-wave readings	Number S-wave readings	Azm. gap	Closest Station	Closest Station with S-wave reading	RMS	Horiz. Error	Vert. Error
	YYYYMM DD	hr:min	sec.	deg. min.	deg. min.		(km)	ML			(deg)	(km)	(km)	(sec)	(km)	(km)
NE	20031225	8:11	22.99	35 42.88	121	4.49	10.4	3.7	67	4	81	13.0	17.8	0.12	.19	.54
SW	20031225	9:34	34.30	35 39.46	121	5.6	6.2	3.4	60	4	109	6.0	17.1	0.12	.23	.71
SW	20031225	9:45	55.37	35 39.57	121	5.71	5.1	4.1 (11)	71	3	111	6.0	16.9	0.12	.20	.61
SE	20031225	11:50	1.55	35 32.62	120	50.77	10.5	4.6 (12)	59	1	35	10.0	42.7	0.09	.18	.55
SW	20031225	14:14	41.17	35 40.42	121	6.38	8.0	3.7	58	3	111	4.0	15.5	0.1	.18	.58
NE	20031225	18:23	31.19	35 42.80	121	5.39	9.9	3.9	72	5	58	7.0	16.4	0.12	.18	.50
SE	20031225	18:31	19.61	35 36.84	120	57.58	7.1	3.2	65	4	78	9.0	16.8	0.1	.18	.62
SE	20031225	19:41	45.96	35 32.21	120	50.16	8.8	3.2	63	3	32	6.0	15.3	0.1	.19	.57
NE	20031225	21:55	23.02	35 43.05	121	3.71	9.2	3.5	67	2	75	13.0	19.0	0.12	.19	.59
SE	20031225	23:25	34.49	35 38.64	120	56.69	6.2	3.2	69	3	62	7.0	20.3	0.09	.16	.56
SE	20031226	2:35	31.81	35 38.07	120	55.57	10.6	3.4	64	4	63	11.0	19.6	0.08	.19	.51
SW	20031226	3:05	29.43	35 39.90	121	6.77	7.0	3.7	39	5	126	4.0	15.2	0.09	.22	.58
SW	20031226	3:45	33.08	35 38.80	121	4.59	2.3	3.6	66	5	94	5.0	19.0	0.12	.18	.51
SW	20031226	10:37	30.74	35 39.77	121	7.09	6.2	3.4	61	4	129	4.0	14.8	0.11	.20	.55
NE	20031226	12:07	37.93	35 41.80	121	2.79	11.7	3.5	65	3	72	11.0	20.4	0.11	.21	.45
SW	20031227	9:19	44.73	35 40.09	121	7.58	8.9	3.4	58	4	136	14.0	13.9	0.09	.21	.62
SW	20031227	12:49	0.47	35 39.49	121	5.19	2.2	3.5	65	4	102	6.0	17.7	0.11	.19	.72
SW	20031227	13:04	49.31	35 39.94	121	6.02	7.6	3.5	67	5	113	7.0	16.2	0.11	.22	.57
SW	20031227	14:22	59.56	35 39.67	121	7.07	2.5	3.6	63	4	129	4.0	14.9	0.12	.23	.69
SW	20031227	14:35	41.12	35 39.68	121	7.64	8.0	3.5	69	3	138	3.0	14.1	0.09	.19	.46
SW	20031227	16:00	11.28	35 39.71	121	7.96	10.0	3.5	65	5	140	14.0	13.6	0.09	.22	.56
SW	20031227	20:01	37.06	35 38.62	121	4.71	2.2	3.5	64	5	96	5.0	18.9	0.11	.18	.55
SE	20031227	20:26	8.61	35 38.30	120	56.43	8.6	3.4	82	5	34	7.0	19.7	0.1	.17	.59
SE	20031228	1:47	45.87	35 36.59	120	53.81	9.5	3.8	78	2	31	8.0	17.9	0.09	.17	.46
SW	20031229	9:05	4.89	35 41.62	121	8.12	10.2	3.8	73	2	73	2.0	29.3	0.11	.20	.40
SW	20031229	15:20	16.81	35 38.89	121	4.47	2.4	3.4	68	3	92	6.0	19.1	0.11	.18	.58
SW	20031229	17:19	19.06	35 38.69	121	4.32	2.3	3.5	68	3	89	5.0	19.4	0.11	.20	.71
NE	20031229	18:05	50.34	35 43.01	121	5.85	9.7	3.8	79	4	89	13.0	15.8	0.12	.20	.48

Cluster	Date	Time (UTC)		Latitude (N)	Longitude (W)		Depth	Mag.**	Number P&S-wave readings	Number S-wave readings	Azm. gap	Closest Station	Closest Station with S-wave reading	RMS	Horiz. Error	Vert. Error
	YYYYMM DD	hr:min	sec.	deg. min.	deg. min.		(km)	ML			(deg)	(km)	(km)	(sec)	(km)	(km)
NE	20031230	6:19	43.87	35 4.300	121	5.36	8.4	3.6	64	2	55	7.0	16.5	0.11	.20	.55
SE	20031230	18:44	5.61	35 31.92	120	48.23	6.9	3.3	71	4	27	9.0	16.9	0.1	.18	.73
SW	20031230	21:17	40.30	35 39.99	121	7.77	9.0	3.6	72	4	138	14.0	13.7	0.09	.20	.52
NE	20031231	4:12	9.41	35 43.09	121	4.06	8.7	3.7	78	4	76	9.0	18.5	0.12	.19	.46
SW	20031231	5:22	1.35	35 40.04	121	5.3	7.4	3.5	70	4	102	7.0	17.2	0.1	.19	.57
SE	20031231	9:46	17.39	35 32.35	120	51.22	8.4	3.3	70	5	38	5.0	14.1	0.08	.18	.53
NE	20040101	11:13	29.10	35 42.67	121	3.19	9.2	3.8	69	3	73	13.0	19.8	0.1	.18	.58
SW	20040102	6:40	20.29	35 38.63	121	4.47	2.1	3.7	62	5	92	5.0	19.2	0.13	.19	.57
NE	20040102	6:44	31.33	35 42.39	121	3.13	8.0	3.4	67	4	56	10.0	19.9	0.11	.17	.57
SW	20040102	10:53	39.53	35 41.71	121	8.59	8.0	3.6	63	3	64	2.0	11.7	0.12	.21	.63
NE	20040103	9:09	48.93	35 42.18	121	3.41	9.9	3.5	75	5	76	12.0	19.4	0.11	.18	.51
SW	20040103	22:28	51.94	35 39.09	121	5.57	1.8	3.4	74	4	110	6.0	17.4	0.1	.19	.53
SW	20040104	5:43	51.07	35 38.92	121	5.07	2.8	3.6	68	3	102	5.0	18.2	0.12	.20	.73
SW	20040104	23:17	15.12	35 40.98	121	6.15	9.9	3.5	80	5	106	9.0	15.6	0.11	.19	.47
NE	20040105	10:24	50.54	35 42.96	121	2.75	7.8	3.5	66	4	50	10.0	20.4	0.12	.19	.49
SW	20040106	6:39	29.69	35 38.21	121	4.37	4.7	3.8	71	3	89	4.0	19.7	0.12	.20	.64
NE	20040106	18:28	37.83	35 43.13	121	5.54	10.9	3.9	79	4	86	12.0	16.3	0.12	.22	.46
SW	20040107	10:54	9.06	35 39.12	121	3.34	7.6	3.5	64	4	77	7.0	20.5	0.1	.20	.58
NE	20040108	0:14	48.81	35 43.44	121	4.68	9.3	3.4	75	2	78	11.0	17.6	0.12	.18	.48
SW	20040109	0:07	33.82	35 40.06	121	6.97	9.9	3.5	73	4	134	15.0	14.8	0.1	.21	.47
SE	20040110	4:09	31.39	35 31.18	120	55.96	3.6	3.5	78	2	88	3.0	7.5	0.1	.17	.40
SW	20040110	9:10	45.08	35 41.91	121	2.48	9.5	3.2	77	4	56	10.0	20.0	0.11	.17	.53
SE	20040114	1:09	15.87	35 34.53	120	47.89	7.5	3.7	73	3	37	11.0	20.6	0.1	.17	.75
NE	20040118	17:57	6.79	35 44.31	121	6.71	9.9	3.2	76	3	46	7.0	14.8	0.12	.19	.48
SE	20040119	11:13	53.76	35 37.94	120	54.98	10.8	3.1	79	4	61	8.0	19.6	0.1	.16	.45
SE	20040119	22:36	44.20	35 38.49	120	56.19	10.7	3.5	84	2	62	6.0	20.2	0.09	.16	.34
SE	20040121	6:25	58.34	35 33.39	120	48.61	10.3	3.5	60	2	45	13.0	18.4	0.09	.18	.65
SE	20040209	14:05	47.25	35 32.87	120	48.69	7.8	3.4	78	5	26	11.0	17.8	0.1	.16	.59

Cluster	Date	Time (UTC)		Latitude (N)	Longitude (W)		Depth	Mag.**	Number P&S-wave readings	Number S-wave readings	Azm. gap	Closest Station	Closest Station with S-wave reading	RMS	Horiz. Error	Vert. Error
	YYYYMM DD	hr:min	sec.	deg. min.	deg. min.		(km)	ML			(deg)	(km)	(km)	(sec)	(km)	(km)
SW	20040210	8:09	21.25	35 40.48	121	6.84	8.9	3.5	74	4	122	11.0	14.8	0.11	.20	.56
SE	20040212	9:27	46.64	35 35.51	120	52.58	7.1	3.8	86	7	32	6.0	17.0	0.1	.15	.48
SE	20040215	2:52	22.64	35 34.64	120	52.43	8.8	3.6	74	3	61	13.0	22.3	0.09	.17	.59
NE	20040217	3:40	18.25	35 43.62	121	4.06	7.0	3.3	76	5	74	7.0	18.6	0.13	.19	.52
SE	20040227	8:33	5.01	35 34.89	120	51.69	4.4	3.8	82	5	30	7.0	16.9	0.12	.17	.86
NE	20040228	4:42	19.16	35 43.20	121	3.72	7.7	3.5	82	5	74	8.0	19.0	0.13	.18	.47
SE	20040305	5:09	16.15	35 34.52	120	50.93	8.6	3.3	70	3	49	7.0	17.1	0.12	.19	.50
SE	20040306	18:22	5.77	35 34.57	120	51.88	8.3	3.4	73	4	58	13.0	16.2	0.09	.16	.64
NE	20040311	7:00	26.95	35 42.33	121	9.07	11.3	3.9	78	4	87	3.0	10.9	0.11	.22	.34
SE	20040313	14:14	18.09	35 32.76	120	52.08	10.6	3.6	64	3	59	10.0	18.8	0.09	.17	.50
NE	20040317	23:53	7.01	35 43.80	121	4.77	9.2	4.5 (13)	82	2	46	6.0	31.0	0.13	.19	.39
NE	20040318	1:41	7.53	35 43.73	121	4.82	7.3	3.0	73	5	48	6.0	17.4	0.14	.19	.52
NE	20040318	10:26	52.46	35 43.39	121	4.71	8.4	3.7	80	5	51	7.0	17.5	0.14	.19	.41
NE	20040318	11:59	36.35	35 43.13	121	3.49	8.4	3.5	69	5	73	8.0	19.3	0.13	.20	.53

* Cluster names are described in Section 5.3; NE=northeast, SE=southeast, SW=southwest

** Numbers in parenthesis next to magnitude 4 values are order of occurrence, as shown in Figure 5-6.